PHOTOCONDUCTING SWITCHES

Photonic control of electronic circuitry via a switching element remains a critical factor in the overall goal of pushing the frontiers of electronic communications and increasing information processing capabilities. Recent advances in the areas of lasers, optical sources, semiconductor-based optoelectronics, and optical fiber technology have all collectively contributed to substantial developments in this field. Photoconductive switching is also becoming increasingly important for high voltage pulsed-power applications, which include (1) high-voltage pulse generators, (2) direct current (dc) to radio frequency (RF) conversion circuits, (3) high-energy pulsed lasers, (4) the generation of ultra-wideband microwaves, (5) high-frequency plasmatrons, (6) impulse radar systems, and (7) frozen waveform generators (1,2). Before the advent of semiconductors, the switching of electric signals was accomplished by gas discharge devices (3). Even today, such devices find limited use in applications requiring very high power generation. However, semiconductor-based switching devices have generally been proven to exhibit far superior performance in terms of speed, compactness, and reliability.

Current solid-state switches fall under two principal categories. The first category is electrically triggered devices that rely on bias-dependent charge injection for conductivity modulations. Typical examples include thyristors, which are current-controlled devices based on a regenerative feedback mechanism arising from internal space-charge layer modulations; metal-oxide-semiconductor field-effect transistors (MOSFET) based on independent control of the internal potentials; MOS-controlled thyristors (MCT); and insulated gate bipolar transistors (IGBT). Several variations of these have also been proposed (4,5). Other current-controlled devices typically based on avalanche breakdown have also been used. Representative examples include the avalanche semiconductor switches (6) and the silicon avalanche shaper (SAS) (7,8). The second category is optically controlled devices, such as the bulk optically controlled switch (BOSS) (9,10), opto-thyristors (11), and optically triggered metal-semiconductor field-effect transistors (12). The optical switches tend to have several inherent advantages and hence are becoming the only true choice for many applications. The benefits include (1) ultrafast response and turn-on times in the subpicosecond regime limited only by the characteristics of the optical trigger; (2) Jitter-free response; (3) superior repetitive rates; (4) Higher-frequency response and controlled wave-shaping capability; and (5) selectivity between multiple optical trigger signals based on the wavelength-dependent response of the photoconductive switches. Furthermore, the wavelength-dependent characteristics can be tuned and altered through a suitable choice of bulk semiconductor materials, through quantum well structures, and through defect engineering. The only obvious disadvantage is the overhead necessary for generating the optical triggering signals.

The central idea behind photoconductive switching is to use a directed and well-controlled beam of photons to switch electrical signals on command rapidly via a suitable semiconductor medium. By modulating the semiconductor impedance via photons, electrical currents can be produced and the signals transmitted to the switch output for subsequent information processing. Generation of the incident optical signals requires suitable lasers capable of generating the requisite wavelength and photon flux with the desired temporal and spatial distributions. Optical fibers often function as the guiding input structure. The biased semiconductor serves as a versatile medium whose conductivity can swiftly be modulated over several orders of magnitude. An electron hole plasma is quickly formed with femtosecond response times as a result of optical band-to-band and band-to-trap transitions as shown by various researchers on the basis of ultrafast pump-probe techniques (13). The electron-hole plasma can be created by any one of the following mechanisms: (1) photoexcitation by an external optical source, such as a laser or a light-emitting diode; (2) electron-beam bombardment to create a plasma; (3) charge injection through device contacts by applying a circuit voltage; and (4) initiation of an internal avalanche breakdown process through either band-to-band or band-to-trap impact ionization. Since photoexcitation is inherently a faster process with superior control, and does not require a vacuum, this is usually the preferred switching option.

The photogenerated carrier mobilities need to be high to produce large photocurrents and efficiently convert energy from the optical to the electrical system. The schematic of a basic photconducting switch is shown in Fig. 1 (14). Typically, a high resistivity, direct bandgap semiconductor such as semi-insulating GaAs (SI-GaAs) or low-temperature grown GaAs (LT-GaAs) is often used as the switch element (2). The switch dimensions are typically determined by the desired on-state resistance, its photon absorption capability, and power dissipation requirements. In the OFF state, the device is in its high resistive state and so effectively holds off an external potential applied to the device. Generally, this hold-off region can be the space-charge region (SCR) of a reverse-biased junction, which is completely depleted of free carriers by the strong external field, or a highly resistive low-doped semiconductor region. While these are the most common, other schemes employing multiple junctions [e.g., optothyristor structures (11)] or those using metal-semiconductor Schottky barriers [e.g., optical MESFETs (12)] have also been proposed. For schemes based on highly resistive low-doped semiconductors, the OFF state is maintained through Schottky contacts, which provide an effective barrier to carrier injection. In the ON state, the conductivity of this region increases dramatically as it becomes filled with an electron–hole plasma.

Historically, photoconductive devices were mainly used for the detection of electromagnetic radiation (15,16). For a long time the measurements were limited to relatively low speeds due to the constraints imposed by the available optical sources and the semiconductor materials. With the development of mode-locked lasers (17) and progress in semiconductor growth and material preparation technology (18), the reliability and applicability of photoconducting device greatly increased. For example, before the discovery of mode-locked lasers, it was not possible to attain carrier densities above 10^{14} cm^{-3} by the conventional light sources. It is now possible to create internal charge densities anywhere in the range of 10^{14} cm^{-3} to 10^{19} cm^{-3}. In addition, tunability of the laser wavelength and intensity has made it possible to manipulate the spatial distribution of the plasma inside the semiconductors. Development of high mobility direct-bandgap materials such as GaAs led to the possibility of high-speed optoelectronics and fast device response. As a result, a new class of high-speed devices based on photoconductive action emerged for various applications including electrical pulse generators and wave shaping, sampling gates, millimeter wave generation and detection, ac to dc conversion, and characterization of device impulse responses (19). The first picosecond laser-induced photoconductivity in high resistivity GaAs for potential switching applications was demonstrated by Auston (20–22). The emphasis for early researchers in this area was on low-voltage, high-speed switching. The high speeds were an important element in increasing the rates and bandwidth for communication and data transfer applications. The subpicosecond laser pulse widths in conjunction with the inherently high electron mobility of the GaAs material were the aspects exploited by researchers (23–28). Other indirect applications of picosecond photoconducting switches came in the development of electro-optic devices such as Pockel cells (29), Ker cells (30), and streak cameras (31). As a natural evolution

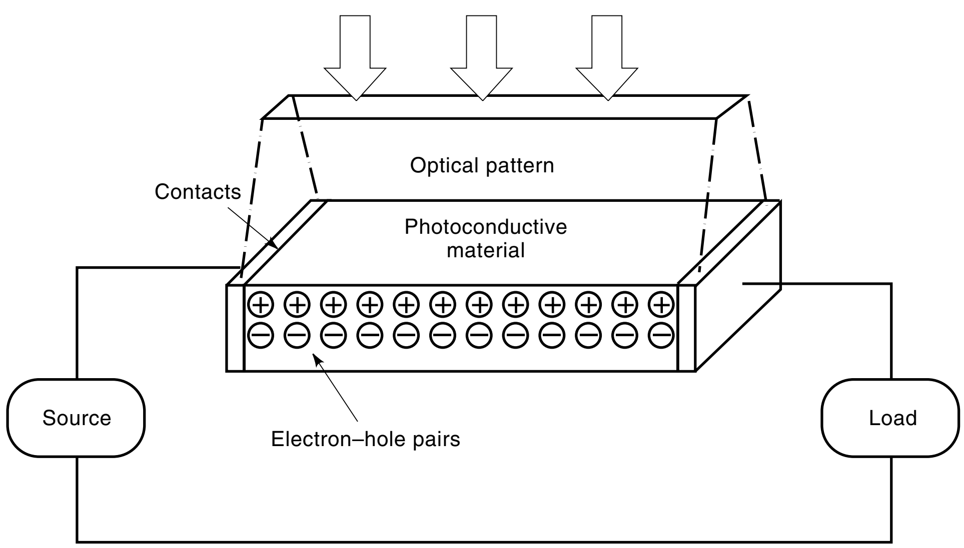

Figure 1. Basic schematic of photoconductive switch (14). A bulk device with photoexcitation incident on the top surface has been shown. The source can be either a dc or an ac signal.

toward attaining even higher electronic speeds based on the photoconductive mechanism, quantum structures have been proposed, fabricated, and analyzed. This is a relatively new development and the reader is encouraged to explore the recent literature (32–37) for specific details. Discussions in this chapter will focus mainly on high-power photoconducting switches given their practical importance.

CHARACTERISTICS OF PHOTOCONDUCTIVE SWITCHES

In general, the following are the desired characteristics of an efficient photoconductive switch:

1. The ability to withstand high electric fields and to have a large breakdown/blocking voltage capability. This is useful for extending the limits for high-power applications.
2. Low leakage currents to preserve a high-impedance OFF state, reduce power losses, and isolate the input circuit from the output side. Such low dark currents would also help reduce noise in such devices.
3. Short turn-on times for superior temporal resolution and higher-frequency operation. Materials such as GaAs and InP having high mobility charge carriers are useful in this regard as the photocurrent response can be made faster.
4. Very low resistance during the conducting ON state to minimize internal heating losses, and the ability to sustain high current densities with a high degree of spatial uniformity.
5. Absence of internal instabilities, such as current filamentation and persistent photoconductivity (PPC).
6. Good thermal conductivity for adequate heat dissipation and the mitigation of second breakdown.
7. Simple structure and ease of fabrication for cost minimization.
8. The absence of internal inhomogeneities, such as traps and defects. Their presence tends to result in a variety of deleterious phenomena, such as PPC, low conversion efficiency, internal heating, increased noise through trapping-detrapping, and the development of spatially inhomogeneous electric fields with current filamentation.

TYPES OF PHOTOCONDUCTIVE SWITCHES

The behavior and electrical response of photoconductive switches, as explained in a later section, are strongly affected by the type of contacts made to the semiconductor. One possible approach of categorizing photoconductive switches, can be based on the type of contact. This leads to the following groups:

1. Devices with dual ohmic contacts. These allow for charge injection into the device from the electrical circuit, in addition to the optical injection. Consequences include the double injection phenomena with possible internal instabilities (38,39).
2. One ohmic (injecting) and one Schottky (blocking) contact. The photocurrents would tend to be lower but with better device stability.

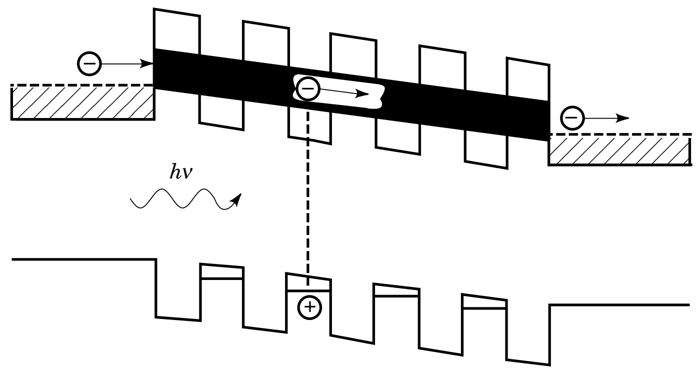

Figure 2. Band diagram of a superlattice photoconductor showing localization of photoexcited holes and miniband transport of electrons (41). The incident photoexcitation energy is shown to be larger than the low band material (typically GaAs), but less than that of the barrier layers (e.g., AlGaAs). The suppression of hole transport reduces noise and increases intrinsic speed.

3. Both contacts Schottky or blocking, leading to a response that is strongly affected by internal carrier lifetimes (40).

Photoconductive switch operation can either be based on the bulk semiconductor properties or utilize characteristics resulting from bandgap engineering to tailor carrier transport. An example might be a photoconductive superlattice structure fabricated from suitable III–V material systems designed to operate at selective wavelengths, as shown in Fig. 2. Use of such superlattices helps suppress the transport of one particular carrier species for greater stability, superior frequency response, and a lower intrinsic noise figure. As shown in Fig. 2, only electrons can contribute to a photocurrent above a threshold wavelength (41). Due to the small dimensions, such structures are not suited for high-power applications.

A classification can also be made on the basis of impurity and defect content of the semiconductor. High-resistivity devices tend to include a high density of defects and midgap states and are referred to as relaxation limited devices. Photoexcitation from the defect levels plays an important role and can lead to PPC and "lock-on" effects (42,43), as discussed later. Such switches are also more prone to device breakdown and current filamentation. Recombination limited devices are relatively defect free and exhibit more stable operation. However, their OFF state impedance and hold-off voltage capabilities are inferior.

SWITCH MATERIALS AND THEIR CHARACTERISTICS

Photoconductive Switch Materials

The choice of semiconducting material is very important for optimizing the electrical response characteristics, its efficiency, and its overall utility. The important parameters are as follows:

1. The material bandgap, which controls leakage currents, the intrinsic carrier concentration, and hence the impedance of the OFF state and places an upper limit on

the operating temperature. It also controls the cutoff wavelength of the input optical excitation. For photoconductive switching, direct bandgap materials are preferred for enhanced conversion efficiency.

2. The breakdown field and dielectric strength, which determine the maximum hold-off voltage. These parameters also provide a measure of the device length necessary to ensure a specific high-voltage blocking capability.
3. The saturated drift velocity, which controls the device response speed and the current density levels.
4. The ionization breakdown threshold.
5. The thermal conductivity, which is a relevant consideration for energy dissipation and enhanced power handling capacity. This is an issue for repetitive high-voltage switch operation.
6. The need to minimize optical losses, such as those encountered during optical fiber transmission, constitutes another important consideration. Since the lowest losses occur at wavelengths of around 1.55 μm, semiconductors having energy gaps in this range are often the materials of choice.

Based on these considerations, GaAs, InP, and other III–V materials have emerged as the semiconductors of choice. However, recently, photoconductive switching for extreme high-voltage applications was demonstrated with SiC (44), ZnSe (45), and Diamond (46) materials. The growth and processing technology for these semiconductors is not as mature [for example, micropipe defects routinely occur in SiC (47)], and so the material quality remains inferior. The conversion efficiencies have been low. The semiconductors are intentionally undoped to achieve low leakage currents and large conductivity modulation capabilities. Much higher resistivities have been attained by using SI-GaAs marginally doped with Si and compensated with deep-level Cu or Fe acceptors (48). The BOSS switch, described in a later section, is a good example. However, this exigency of fabricating high-resistivity, semi-insulating material profoundly affects the transport characteristics and electrical response behavior. The relatively large density (as at least as compared to other electronic devices) of impurity and defect states produces the following effects:

1. A multitude of emission and trapping time constants influence the recombination dynamics and can be observed through the multiexponential decay in deep-level transient spectroscopy (DLTS) experiments.
2. The midgap states produce larger mobile carrier densities as a result of trap-to-band transitions. One of the immediate effects is PPC.
3. The transport becomes akin to that found in “relaxation-time semicondutors” rather than the usual “recombination-time semiconductors.”
4. Trap-to-band impact ionization and slow carrier emission from filled deep levels leads to a slow photoconductive decay.
5. There are enhanced noise spectra. However, as the switching signals have relatively large magnitudes, this is not a significant issue.

Deep-Level Investigations

The SI photoconductive switches usually contain deep-level impurities, which requires careful characterization through techniques such as DLTS (49), photo-induced current transient spectroscopy (PICTS) (50), transient photo hall (51), and the thermally stimulated current (TSC) methods (52). PICTS is used for highly resistive switches, as their capacitance values are unsuitably low for DLTS measurements. The photo hall and TSC techniques distinguish between electron and hole traps. The experiments yield the density, energy level, electron, and hole capture cross sections for all states in the forbidden zone. This information is important for determining the OFF state conductivity, the turn-off and decay times, and the wavelength dependence. It can also be used for simulations of transport, the current transient response, and predictions of internal electric field and carrier density profiles. Typical data obtained for SI-GaAs doped with Si and compensated by Cu dopants from DLTS and PICTS measurements is available in the literature (53). Of particular significance are the multiple levels associated with the Cu impurity, the DX complexes, and the disparity between the trapping cross sections for electrons and holes, which is indicative of capture at a charged site via a screened Coulomb-type potential. Some of the multiple levels have been known to produce both acceptors and donorlike behavior (54). In the BOSS switch, however, this multiplicity is used for independent optical turn-on and turn-off.

Dark Current-Voltage Characteristics

The dark current–voltage characteristics of a photoconductive switch describe the state of the switch prior to being optically turned on. In some switch designs, the maximum voltage that can be applied to the switch is limited by an electrical breakdown across the surface of the semiconductor material. In most designs, however, the maximum electrical operating characteristics of the switch are limited by the bulk conduction properties of the semiconductor material. Many methods have been developed to characterize a semiconductor material with respect to its doping, defects, or traps within the bandgap of the material and thermal charge carriers. The particular method, which is of interest for this discussion, is the use of space-charge limited (SCL) current injection. Mott and Gurney first addressed the theory of SCL currents in solids in 1940 (55) and developed what is now called the trap-free square law (TFSL). The following addresses the impact of deep levels (or traps) on the dark, or non-laser-illuminated, current-voltage characteristics of bulk photoconductive switches.

Conduction Theory of Single-Carrier Injection. For the discussion in the following subsections, only single-carrier (electron) injection will be considered. This analysis also ignores any spatial variations in the quantities by considering only their respective average values.

The Trap-Free Square Law. To derive the TFSL, it is first assumed that there are no thermal free carriers ($n_0 \approx 0$) and that there are no trapping states ($n_{tj} \approx 0$). The electron current density is given by

$$J = e\mu n_i E \tag{1}$$

where e is the charge of an electron, μ is the electron mobility (which in this case is considered to be constant), E is the applied electric field, and n_i is the injected electron concentration. These electrons remain in the conduction band and result in a negative space charge. Combining Eq. (1) with Poisson's equation,

$$\left(\frac{\epsilon}{e}\right)\frac{\partial E}{\partial x} = n_i \tag{2}$$

where ϵ is the material permittivity, yields

$$\frac{J}{\mu\epsilon} = E\left(\frac{\partial E}{\partial x}\right) \tag{3}$$

Using the boundary condition, $E(0) = 0$, where $x = 0$ at the cathode (which effectively assumes that the contact metal-semiconductor work function difference can be neglected), leads to following potential $V(x)$:

$$V(x) = \left(\frac{8J}{9\epsilon\mu}\right)^{1/2} x^{3/2} \tag{4}$$

Letting $x = L$ at the anode and $V = V(L)$ yields the TFSL result,

$$J = \left(\frac{9}{8}\right)\epsilon\mu\left(\frac{V^2}{L^3}\right) \tag{5}$$

The Influence of Thermal Free Carriers. When thermal free carriers are taken into account, there is considerable deviation from the TFSL. Thermal-free carrier concentration (n_0) in excess of the intrinsic concentration results from the thermal ionization of uncompensated donors or acceptors in p-type material) located in the bandgap of the material. When the crystal lattice is in thermodynamic equilibrium (TDE), the concentration of free carriers results from a dynamic balance between thermal excitation from impurity levels within the bandgap and their subsequent recapture back into the impurity levels.

Since photoconductive materials are typically undoped and often contain midgap levels, the semiconductor is nondegenerate, with a Fermi level (F_0) lying several kT below the conduction band. The carriers can then effectively be characterized by a Boltzmann distribution function, and the free carrier concentration (n_0) becomes

$$n_0 = N_c \exp\left[\frac{F_0 - E_c}{kT}\right] \tag{6}$$

where N_c is the effective density of states in the conduction band and n-type material has been assumed. Therefore, for low voltages we now expect the current (J) to follow Ohm's law,

$$J = en_0\mu\left(\frac{V}{L}\right) \tag{7}$$

Even though there will be charges injected into the semiconductor at low voltages, this injected charge (n_i) will not cause a departure from Ohm's law until the condition, $n_i \approx n_0$, is met (39).

Charge Carrier Trapping Effects. When there are traps present in the bulk of the semiconductor, the current is greatly reduced as a result of the capture of injected carriers' empty traps. The amount of excess charge that can be supported in the bulk at an applied voltage V is a function of the geometric capacitance C_0 and is independent of whether the excess charges are mobile or exist in trapped states.

In the presence of an external field applied across the switch, it can be assumed that the balance between free and trapped electrons is altered only by electron injection at the boundaries. The new free-electron concentration (n) brought about by injection produces a new quasi-Fermi level (F). Under injection conditions, the densities become

$$n = n_i + n_0 = N_c \exp\left[\frac{F_0 - E_c}{kT}\right] \tag{8}$$

and

$$n_t = n_{ti} + n_{r0} = \frac{N_t}{1 + \frac{1}{g}\exp\left[\frac{E_t - F_0}{kT}\right]} \tag{9}$$

respectively, where N_t is the concentration of traps, n_i is the average excess free-electron concentration, n_{ti} is the average excess injected trapped-electron concentration, and n_{t0} is the density of filled traps at a level E_t within the bandgap given by

$$n_{t0} = \frac{N_t}{1 + \frac{1}{g}\exp\left[\frac{E_t - F_0}{kT}\right]} \tag{10}$$

with g the ground state degeneracy for the traps. The degeneracy equals 4 for donor levels and 2 for acceptor levels.

A trap state is usually considered shallow if the quasi-Fermi level F lies below E_t or $[(E_t - F)/kT] > 1$. Under these conditions, the preceding equations lead to

$$\frac{n}{n_t} = \frac{N_c}{gN_t}\exp\left[\frac{E_t - E_c}{kT}\right] = \Theta \tag{11}$$

where Θ is independent of the injection level if the trap remains shallow. A shallow trap can thus have a substantial effect on SCL current injection if $\Theta \ll 1$. Substituting $n = n_t\Theta$ yields the shallow-trap square law relation given by

$$J = \left(\frac{9}{8}\right)\Theta\epsilon\mu\left(\frac{V^2}{L^3}\right) \tag{12}$$

For a deep trap, where F lies above E_t, the condition $[(F - E_t)/kT] > 1$ holds. This then leads to the following expression for the hole occupancy of the trap at thermodynamic equilibrium:

$$p_{t0} = N_t - n_{r0} = \frac{N_t}{1 + g\exp\left[\frac{F_0 - E_t}{kT}\right]} \tag{13}$$

It is often assumed that as the injected free-electron concentration (n_i) becomes comparable to n_0, the corresponding shift of the quasi-Fermi level is sufficient to fill the deep traps (39).

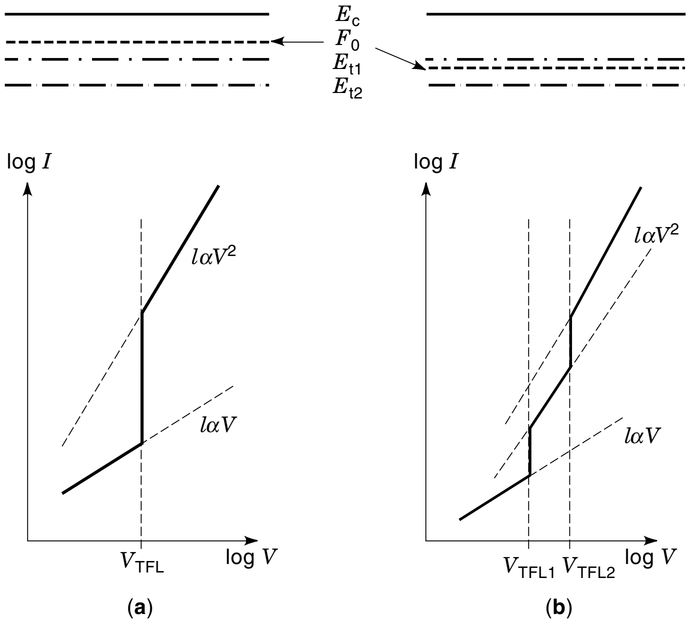

Figure 3. Models of dc current-voltage (I–V) characteristics for semiconductor materials containing deep levels. E_c is the conduction band, F_0 the Fermi level, while E_{t1} and E_{t2} are two arbitrary trap levels. With increasing current, the Fermi level moves up toward the conduction band and the trap levels progressively begin to fill. This leads to strong current enhancements.

This assumption ignores the asymptotic behavior of trap filling by assuming the trap to be completely filled at a critical threshold voltage V_{TFL}. In the experimental curves, however, the transition is seen to occur more gradually. Therefore, the condition $n_i \approx n_0$ corresponds to the voltage V_{TFL} required to fill the trap. This yields the following expression for V_{TFL} in terms of p_{t0}:

$$V_{\mathrm{TFL}} = \frac{Q_{\mathrm{TFL}}}{C_0} = \frac{ep_{\mathrm{r0}}L}{C_0} = \frac{ep_{\mathrm{r0}}L^2}{\epsilon} \tag{14}$$

where Q_{TFL} is the charge injected into the bulk at V_{TFL} and C_0 is the geometric capacitance of the sample.

It is easiest to determine the behavior beyond V_{TFL} by comparing the current density at V_{TFL} to that of $2V_{TFL}$. Because $Q = CV$, when V is doubled the injected charge is also doubled. This additional charge will then appear in the conduction band and is equal to $(ep_{t0}L)$. Now assuming that $n(V_{TFL}) \approx 2n_0$, the ratio of the two current densities becomes

$$\frac{J(2V_{TFL})}{J(V_{TFL})} \approx \frac{p_{\mathrm{r0}}}{n_0} \tag{15}$$

From Eq. (15) it becomes clear that by doubling the voltage, the current density can increase by several orders of magnitude.

Figures 3(a) and 3(b) illustrate two possible direct current (dc) current-voltage (I–V) characteristics for a material that contains two traps. In Fig. 3(a), both traps are deep, with E_{t1} being full at thermal equilibrium. As the voltage is applied, the quasi-Fermi levels move up in the bandgap until $n_i \approx n_0$, at which time V_{TFL} is reached. Up to this point the I–V characteristics are expected to be ohmic. As the voltage is further increased, the current would increase several orders of magnitude by an amount proportional to (p_{t0}/n_0). After this jump the current may merge with the trap-free square law. It is possible to ascertain whether this square law is due to a shallow trap or a trap-free condition provided the material electron mobility is known.

In Fig. 3(b) we have the condition that one trap (E_{t1}) is below F_0 and the other (E_{t2}) is above F_0. The transition at V_{TFL1} will result from the deep trap, as was the case in Fig. 1(a). However, because of the shallow trap (E_{t2}), the jump is reduced as some of the injected charge would be used to fill E_{t2}. With increasing voltage, the current should follow the shallow-trap square law until the quasi-Fermi level reaches the energy of E_{t2}, beyond which another near vertical transition would occur at V_{TFL2} up to the TFSL (56).

From the preceding discussion it is clear that for single-carrier injection the current is limited by the space charge in the material. Therefore, when the I–V characteristics are plotted logarithmically, the measured data will be confined within a triangle bounded by three limiting lines. These lines are Ohm's law, where $I \propto V$; the TFSL, where $I \propto V^2$; and the line defined by Eq. (14), which determines the voltage where the current steeply rises up to the TFSL.

We next illustrate, in Fig. 4 (57), the dramatic effect that deep levels have on the dc I–V characteristics of a SI-GaAs device sample configured with ohmic contacts on opposite sides of a 0.05 cm thick sample. The resistivity of the SI-GaAs sample was found to be 3.3×10^7 Ω-cm. In this figure, the open squares indicate the current density that was measured with a dc bias voltage, and the closed circles indicate the current density measured with a pulsed bias voltage. The time development of the dark current will be discussed in the next section. From Fig. 4 we see that the V_{TFL} equals about 70 V, which from Eq. (14) results in a value for p_{t0} of 2.0×10^{11}

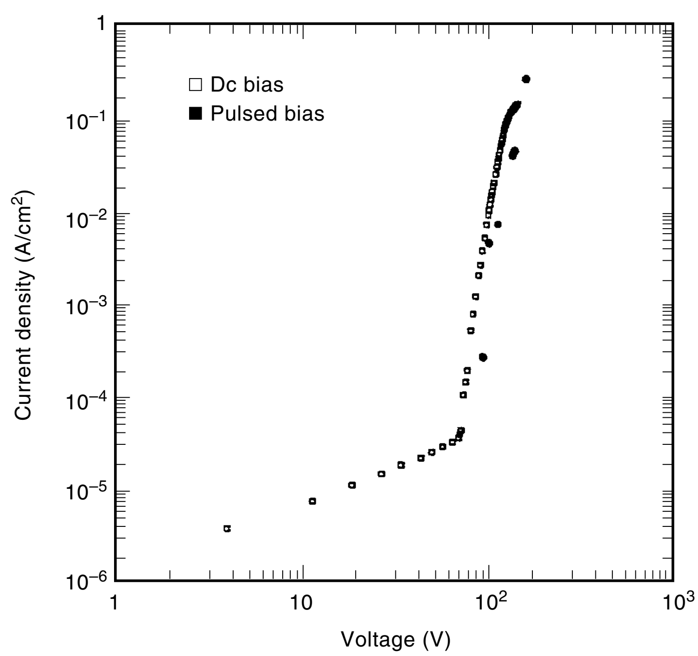

Figure 4. Dark current density versus applied voltage for a 0.05-cm thick SI-GaAs sample. The experimental sample contained deep levels. The effect of trap filling was clearly evident from the dramatic increase in the current at about 70 volts.

cm^{-3}. Determination of the trap concentration, N_t, requires information on the positions of the Fermi level and the trap position within the bandgap. To get this information one can return to the Ohmic portion of the I–V characteristics in Fig. 4 and use Eq. (7) to determine the free-carrier concentration of $n_0 \approx 3.75 \times 10^7$ cm^{-3}. This leads to a value of $E_c - F \approx 0.6$ eV at 300 K. Information on the position of the electron trap cannot be obtained from Fig. 4 explicitly. However, if we assume that the dominant trap in SI-GaAs is the EL2 level, we can use an energy of $E_c - E_t = 0.825$ eV (58). Based on the Fermi and trap energies, the density N_t can be determined. Here the data yield a density $N_t\{\mathrm{EL2}\} = 2.4 \times 10^{15}$ cm^{-3}, which is within a factor of three of the value normally quoted for SI-GaAs (59).

Temporal Development of the Dark Current. The previous section discussed the current-voltage characteristics of semi-insulating devices, where the charge occupations of the deep levels in the bulk material were allowed to reach a steady state. Here we discuss the transient material response to a pulsed bias voltage. This transient response occurs with characteristic time constants that are related to the deep levels controlling the electrical properties of the material. The transient dark current is particularly important to the discussion of bulk photoconductive switches because they are normally biased with a voltage pulse rather than a constant voltage value. Pulsed bias voltages are used because, as we will see, the ability of a bulk semiconductor to hold off an applied voltage is much greater when voltage is applied for a short time.

For this discussion we will again use SI-GaAs as a representative example of a bulk material often used in photoconductive switches. To investigate the temporal characteristics of the dark current, a hard-tube pulse generator was constructed that could apply up to a 3 kV pulse with a 1 ms duration, or up to 1 kV for a pulse duration of 500 ms. The use of a voltage pulse allowed higher voltages to be applied across the sample than would be possible with a dc bias voltage because it reduced the amount of heating caused by high dark currents. The circuit consisted of a storage capacitor that was charged to the desired voltage and then discharged through a resistance that was in parallel with the sample. The switch used to control the pulse width was an RCA 6293 beam-power-amplifier vacuum tube with a maximum anode voltage of 3.5 kV.

We will first discuss results for a SI-GaAs sample with a thickness of 0.065 cm and a bulk resistivity of 6×10^6 Ω-cm. An example of a typical voltage and current waveform is shown in Fig. 5 (60). It was found that when the voltage was first applied, there was an initial current spike that was attributed to the displacement current. After the displacement current, the dark current remained very low for a delay period and then monotonically increased up to a saturation value. We call this delay before the increase of the dark current the "onset time," and it was found to be a strong function of the amplitude of the applied voltage pulse, as shown in Fig. 6 (57). In Fig. 5, the onset time was about 900 μs and the time required to get to the saturation value was about 2.9 ms for an applied voltage of 200 V. This effect was previously found to occur on p–SI–n structures when the p and n regions were epitaxially grown on a SI-GaAs substrate (61). This effect was also later studied by Roush et al. (62) in copper-doped SI-GaAs.

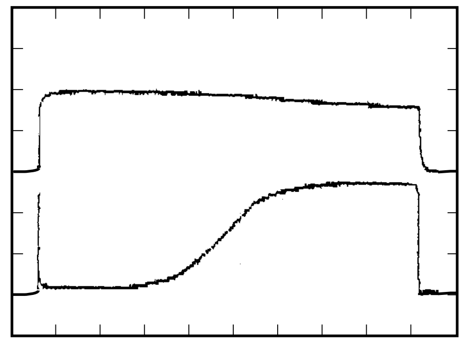

Figure 5. Temporal development of the switch dark current. The sample resistivity was 6×10^6 Ω-cm. The experimental data (60) shows a delay in device current primarily associated with the trap-filling time.

Double pulse experiments were also conducted to determine the recovery of the material after the removal of the voltage. As expected, the circuit current in Fig. 5 terminates with the voltage pulse. However, when a second voltage pulse is immediately reapplied to the device, the onset time is considerably shorter. In fact, at room temperature it normally took more than a second delay between pulses for the initial onset time to be measured. This effect was also investigated by Brodovoi et al. (63), who found that for SI-GaAs : Cr material at 77 K, the material did not return to its initial resistivity for two to three hours after the voltage was removed. However, if the sample temperature was raised back up to room temperature, the sample again became highly resistive. All of these results strongly indicate the effects of carrier trapping and emission in the bulk of the material.

The onset time was not only found to be a function of the applied voltage and temperature but also the deep-level configuration of the material. This was discovered when the same experiment was conducted on SI-GaAs : C material with a re-

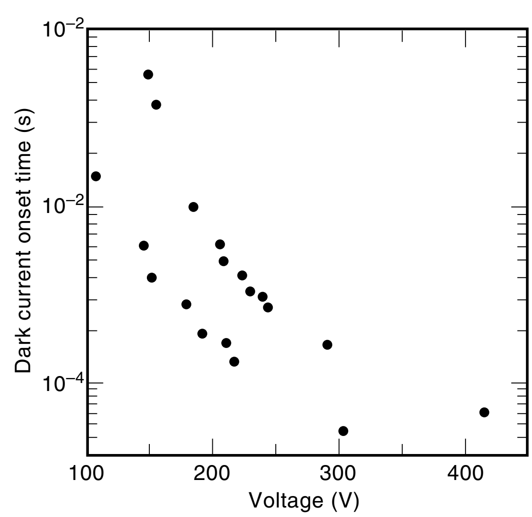

Figure 6. Dark current onset time versus applied voltage. The experimental data (57) shows faster trap filling leading to lower onset times with increasing voltage. The higher currents at the higher voltages help in filling traps faster.

sistivity of 3×10^8 Ω-cm. For this material, at an applied voltage of 650 V, the onset time was found to be 120 ms and the saturation time was about 320 ms at room temperature. Therefore, this material had an onset time that was more than two orders of magnitude longer than the 6×10^6 Ω-cm material at a factor of 3 higher bias voltage—again indicating the influence of deep levels and their charge occupation in the bulk material.

We next compare the results obtained with a dc bias to those obtained using a pulsed bias. It was found that the saturation current measured with a pulsed bias was in good agreement with the current measured under steady-state conditions. The agreement is shown in Fig. 4 for an as-grown SI-GaAs material with a resistivity of 3.3×10^7 Ω-cm. In this figure the open squares indicate the current density that was measured with a dc bias, and the closed circles indicate the saturation current density measured with a pulsed bias.

Similar results were obtained for the SI-GaAs : C sample, as shown in Fig. 7. In this figure the open circles correspond to a dc bias voltage, while the solid squares indicate the saturation current obtained with a pulsed bias. Here again the saturation current seems to fall in line with the dc bias measurements. Also shown in Fig. 7 are the results of a pulsed bias experiment where the dark current was measured after 1 ms (open squares). It is interesting to note that the difference between the pulsed currents (open squares) and saturation currents (closed squares) can be as much as three orders of magnitude. It is expected that the vertical transition in the pulsed bias curve would shift more to the right as the voltage pulse duration is decreased.

We will now give a qualitative explanation of the internal material physics when a voltage pulse is applied. The temporal development of the dark current (Fig. 5) can be qualitatively explained with the use of a model that contains two deep levels. One level is an electron trap (possibly EL2) and the other level is a hole trap (possibly Cr). During the initial part of the voltage pulse, electrons injected at the cathode are trapped by EL2. These trapped charges are immobile and constitute a negative space charge. Recall that the space charge that limits the current in a material is independent of whether the space charge is free or trapped. Also during the initial phase of the dark current, holes are being injected at the anode contact, which is less efficient at injecting minority carriers than majority carriers. After being injected, these holes subsequently drift toward the cathode until they are trapped in the Cr level with a time constant that is dependent on the hole capture cross section, the concentration of the Cr level, and the hole concentration in the material. As the holes are trapped, they will compensate the negative space charge contained in EL2 and therefore allow more electrons to be injected at the cathode. Once the hole trap is full, a steady-state condition will be reached. The value of the current that is measured at this point should be equivalent to the value that is measured when a dc voltage is applied.

The increase in the onset time for the case of SI-GaAs : C material can also be explained with the two-level model discussed previously. The EL2 and Cr levels are both located near the middle of the bandgap in GaAs. The carbon level is located very close to the valence band and is a shallow acceptor. The role of carbon in SI-GaAs is to lower the Fermi level and therefore decrease the equilibrium occupation of EL2. This electrical compensation of EL2 results in a higher-resistivity material. Because the occupation of EL2 is reduced, the amount of time required to fill the trap is increased. Therefore, a longer onset time is measured because the injected electrons will not stay in the conduction band long enough to carry a current if there are still unoccupied electron traps.

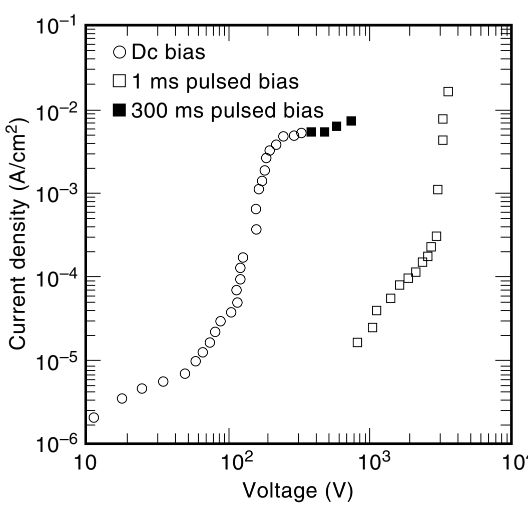

Figure 7. Dark current density versus applied voltage for a 0.05-cm thick SI-GaAs : C sample. The curves clearly show that significantly lower currents can result at the same voltage for lower pulse durations. This effect is due to incomplete trap filling for the lower pulse durations.

Fast-Neutron Irradiation

The effects of neutron irradiation on semiconducting materials have been studied for many years (64). A more recent effort has concentrated on the reduction of minority carrier lifetime in GaAs through fast-neutron irradiation. The principal purpose is to create internal defects within the material through the process of elastic nuclear scattering between incoming fast neutrons and the host lattice atoms. Typically, the incident neutron suffers at most one collision, resulting in the displacement of either a Ga, As, or impurity atom. The recoil energy is large enough to initiate a displacement cascade, with each primary knock-on atom creating several defects.

Such neutron-initiated defect formation has been used to quench the lock-on or persistent photoconductivity phenomena commonly observed under high-voltage conditions in optically activated switches. The recombination centers and defects formed due to the neutron treatment provide an additional channel for excess carrier removal. This helps limit internal charge densities and the currents. Device dark currents are also reduced, thus affecting the dc I–V characteristics. These results are from experiments performed at the Sandia National Laboratory. Finally, the effect of such irradiation on the switching behavior of SI-GaAs BOSS samples (65) was also investigated. Clearly evident was the quenching of PPC with increasing neutron dose, as discussed in more detail later in this article. Other types of irradiation have also been used to reduce the minority carrier lifetime in ultrafast photoconductive switches (66).

THEORETICAL CONSIDERATIONS

Issues and Problem Areas

While photoconductive switches are commercially available for low-voltage high-speed operation, extending their capabilities to the kilovolt range and beyond has presented a challenge. The primary issues and deleterious effects encountered in photoconductive switching are as follows:

1. Persistent photoconductivity and the appearance of a lock-on current mode.
2. Surface flash-over and premature breakdown. Immersion in suitable high-dielectric liquids is often used as a preventive measure of surface flashover.
3. Current filamentation and physical damage originating at the contacts. This is accompanied by infrared luminescence as demonstrated through time-resolved imagery (67). The luminescence is indicative of the onset of direct carrier recombination following strong internal impact ionization.

Lock-on is a persistent photoconductivity (PPC) effect. It leads to a failure of the switch to open and revert back to a high impedance state following the termination of external photoexcitation. Current filamentation and physical damage have often been observed to follow as a natural consequence. Excessive semiconductor heating leading to thermal runaway can also occur. Infrared imaging suggests that the damage is caused by high electric fields at the contacts. Typical images of device damage and high-voltage breakdown during switch operation reveal that the critical failure regions are concentrated near the contacts. Such phenomena are voltage dependent and exhibit a threshold. The following salient features have been observed for the lock-on mode:

1. It occurs only when the bias voltage is greater than a certain minimum value. The corresponding average electric fields range from 3.5 kV/cm to 15 kV/cm, depending on the material, preparation, and temperature.
2. The lock-on condition only occurs after optical triggering.
3. The lock-on state appears to be a precursor to potential device breakdown.
4. Strong internal gain is observed, leading to optical conversion efficiencies that are almost three orders of magnitude higher than at low voltages.

Qualitative Physics of Switch Failure

Persistent photoconductivity has been widely observed in a variety of materials, including the III–V and II–VI compounds (68–71), Si (72) and GaN (73,74). The phenomenon is not limited to bulk devices but also occurs in modulation doped structures and heterojunctions. Carrier density increases of up to four orders of magnitude have also been associated with this phenomenon (75). In all cases, the PPC has been linked to the presence of deep traps. This is especially relevant to photoconductive switches, since the materials often contain a high level of intentional traps and deep-level impurities. In addition, GaAs, a popular material for photoconductive switches, contains DX centers that also contribute to the mix of deep-level states. These deep levels are located away from the center of the Brillouin zone and are either at the L or the X symmetry points. This has a profound effect on the recombination times of mobile carriers.

Persistent photoconductivity can perhaps be best understood by considering the photogeneration process in a high-resistivity material. Carriers are generated from all of the deep levels and placed in the L or X valleys. This process is in addition to the ongoing direct valence-to-conduction band transitions and can lead to mobile carrier densities that are substantially larger than those in trap-free materials under identical conditions. Following initial photoexcitation from deep levels, the carriers predominantly populate the lowest Γ valley through internal scattering and energy/momentum randomization. Such carriers then tend to be relatively long lived as the Γ–L and Γ–X recombination processes are indirect and require the presence of mediating phonons.

The preceding simple model, which relies on deep traps alone, is inadequate and incomplete to account for all the observed effects in high-voltage photoconductive switches.

1. For instance, the PPC and lock-on phenomena are observed only above certain critical applied bias levels. Hence, it appears necessary to invoke an appropriate field-dependent phenomenon. Such a field-dependent mechanism cannot be associated with the trapping dynamics of carriers into the trap states, as this process actually gets enhanced with increasing field. This follows because electrons at higher fields are able to populate the satellite valleys and upper bands, thus opening up the possibility of direct transitions into trap states. On the basis of field-dependent carrier trapping alone, one would expect the opposite effect of reducing PPC through enhanced carrier removal.
2. Though the indirect recombination route is slow in trap-dominated semiconductors, the channel of charge removal from the system through carrier sweep-out and conduction outflow still exists. The presence of PPC and lock-on thus suggests that a continuous injection from the contacts must replenish the internal mobile charge, thereby maintaining a high carrier density. Furthermore, such an injection process has to be field dependent to account for the observed bias-dependent lock-on phenomena.

Once the importance of metallic contacts is recognized, it becomes simple to account for the observed field-dependent lock-on threshold. An explanation for current filamentation and severe damage at the contacts (67) reported in various experiments on high-voltage photoconductive switches follows from details of the carrier injection process. In general, transport at the contacts occurs via the following mechanisms (76):

1. thermionic emission over the potential barrier between the semiconductor and the metal.
2. quantum mechanical tunneling, both direct and indirect. The latter can be facilitated through the existence of states within the forbidden gap and is a highly field-dependent phenomenon.
3. Recombination within the space charge layer in the vicinity of the contact.

Of these, the tunneling process gives rise to sharp injection enhancements provided that the fields at the contacts exceed a critical threshold. Furthermore, such injection strongly depends on the value of the effective barrier height at each location of the contact-semiconductor interface. Hence, if the barrier potential were to be spatially nonuniform along the transverse direction, one would then get nonuniform injection from the contacts. The existence of such spatial, in-plane, barrier nonuniformities at the contacts has been conclusively demonstrated in the literature (77–79). For example, previous work at low voltages on metal-semiconductor Schottky contacts has shown that such nonuniformities can affect the "ideality factor" of Schottky diodes and hence alter the current-voltage characteristics (80). At the higher voltages the spatial nonuniformities play an even greater role, with the field-dependent current injection leading to nonuniform filamentary currents at the contacts.

An optical pulse on the photoconductive switch serves to enhance the electric fields at the contacts as a result of charge separation and internal polarization. Strong injection from the contacts can then be expected to occur provided that the enhanced contact fields were sufficiently above the threshold limit. It thus becomes clear that the field-dependent injection efficiency is then controlled not only by the incident photoexcitation intensity but also by the value of the applied bias. A higher bias, for example, yields a higher initial field at the contacts prior to photoexcitation. Consequently, a lower optical intensity would be required to surpass the threshold field and trigger strong injection. This strong injection would then lead to PPC, and even filamentation if the contact barrier potential were to be spatially nonuniform. Such a dependence of the photointensity on filamentary breakdown has been experimentally observed (81). The preceding scenario suggests that control of the detrimental effects would require fabrication of "blocking contacts," better spatial homogeneity, and a decrease in the carrier lifetime. The use of magnetic fields and neutron bombardment might be options in this regard. Finally, electric fields at the contacts could be lowered by utilizing curved geometries and avoiding sharp corners.

The role of contact injection can easily be demonstrated through numerical two-dimensional (2-D) simulations. Such calculations carried out for an SI-GaAs photoconducting switch with a simple 10 μm square geometry are discussed next. The surface area was chosen to be 10^{-4} cm^2, and the contacts were assumed to be on the top and bottom faces diagonally across from each other. A simple 50 Ω resistor was taken to be in series with the photoconductive switch. The SI-GaAs material was assumed to have a marginal n-type donor density of 10^{15} cm^{-3} and a trap concentration of 10^{16} cm^{-3}. The trap level was set at 0.6 eV from the conduction band, with electron and hole capture cross sections of 10^{15} cm^2 and 10^{17} cm^2, respectively. These values are consistent with observations for SI-GaAs material, while all other transport data were taken from Ref. 65 and sources quoted therein.

Simulation results for the photocurrent with and without the contact tunneling process are shown in Fig. 8 in response to an applied voltage waveform consisting of a 1.0 ns ramp followed by a 100 V bias. A constant photoexcitation pulse was assumed to illuminate the semiconductor continually between 10 ns and 15 ns. Initial conduction lasting up to 1.0 ns for both cases is the displacement current associated with the external voltage ramp. The rise at about 10 ns follows the optical pulse initiation. The dip at about 12 ns results from internal polarization effects and the gradual decrease in the device voltage due to the 50 Ω voltage resistive drop. The subsequent increase is simply the result of enhanced electron velocity at the lower fields characteristic of GaAs material. Finally, after the termination of the optical input at 15 ns, the photocurrent is seen to decay if the contact tunneling process is not included. However, with tunnel injection two primary differences can be seen: (1) The current magnitude is larger, and (2) the photocurrent does not appear to decay upon the termination of the photoexcitation pulse at 15 ns. This clearly demonstrates the lock-on phenomena and its link with strong field-dependent contact injection.

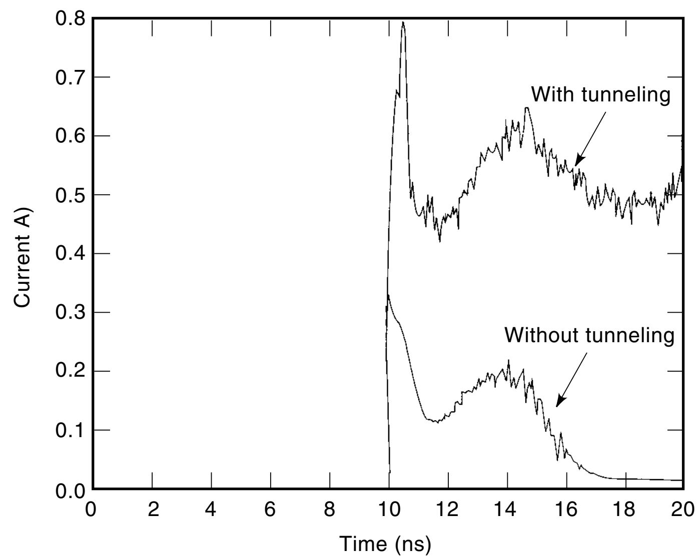

Figure 8. Simulation results showing the response of an SI-GaAs switch to an external 5.0-ns photoexcitation pulse initiated at the 10-ns time instant. Lock-on is predicted only when carrier tunnel injection at the contacts is taken into account. This simulation result brings out the role of high field electron injection at the cathode.

The presence of moving high-field domains arising from an inhomogeneous defect density distribution in the III–V photoconducting switch materials can be another potential source for instabilities. As Gunn first pointed out (82), a local inhomogeneity near the cathode can function as the nucleation site for a high field domain. This domain formation is associated with the intervalley k-space transfer of electrons at fields (83). Such domains propagate toward the anode, subjecting various regions of the semiconductor material to high internal electric fields. There can then be two routes to instability: (1) The domain field may be large enough to cause strong impact ionization through the band-to-band and trap-to-band processes; or (2) a more gradual increase in the carrier density may result as the domain sweeps past regions containing defects and impurities. For such a process, though, the characteristic carrier emission times need to be smaller than the domain transit time, a condition that is easy to meet for deep defect levels. The effect, however, can be cumulative as the carrier densities can be substantially increased after several transit cycles. Hence, for a constant device voltage, both the current and domain field increase dramatically as the domain width is reduced. This inherently gives rise to an unstable

S-shaped current-voltage device response characteristic (84), which can be potentially unstable.

PHOTOCONDUCTIVE SWITCH SYSTEMS

Some of the more common photoconductive switch systems are briefly discussed in this section to bring out the various concepts used and their relative advantages. We limit our discussion here, however, to the use of photoconductive switches in high-power applications. We will discuss devices that remain closed after the application of a short laser pulse, devices that remain closed only during laser illumination, and devices that are closed by the application of one laser pulse and subsequently opened by applying a second laser pulse of a different wavelength. A review of high-powered photoconducting switch concepts appears in the text *High-Power Optically Activated Solid-State Switches,* edited by Rosen and Zutavern (85).

Lateral Photoconductive Switches

We begin our discussion of switch concepts by introducing the lateral switch geometry as shown in Fig. 9. Both the contacts are in the same plane and lie on opposite sides of the common face. This geometry is often used for switches that are operating in either the linear mode or the nonlinear filamentary mode of operation. A similar configuration would have the two contact metalizations located on opposite faces of the semiconductor crystal. The switch active region then corresponds to the distance that the two contact edges are offset from each other. This latter geometry is used to increase the hold-off voltage of the switch by minimizing the potential of surface flashover. The lateral switch geometry is also convenient for electrically connecting the device to a high-bandwidth microstrip circuit. Alternatively, the lateral switch can also be integrated with the microstrip line, as shown in Fig. 10.

Typically, when a lateral switch is operated in the linear mode, the active region of the device is flooded with photons from a relatively high-power laser (86). The wavelength of the laser system is normally selected to be slightly below the bandgap energy of the semiconductor material. Photons can then penetrate deeper into the bulk of the material, where they will create conduction electrons and holes nearly uniformly. One electron hole pair produced for each photon absorbed characterizes the linear mode. The uniform illumination can result in nearly uniform current conduction through the switch material and result in relatively long lifetimes in terms of total number of switching events. Linear switching requires substantial laser illumination, on the order of 10 μJ/cm^2 to 1 mJ/cm^2, to obtain a satisfactory switch resistance of less than 1 Ω (86).

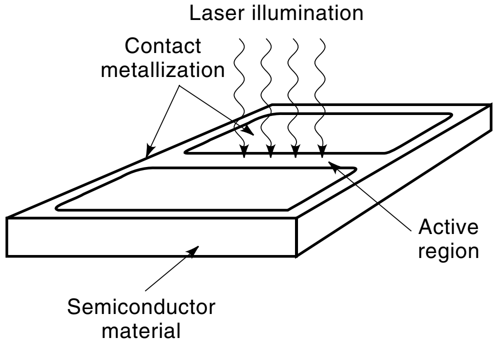

Figure 9. Lateral photoconductive switch geometry. For this typically simple geometry, the thickness is chosen to approximately equal the laser absorption depth to maximize efficiency.

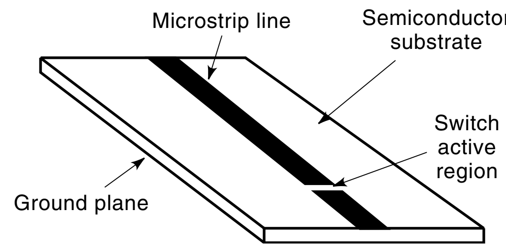

Figure 10. Lateral switch geometry integrated into a microstrip line using the same material. Such integration allows coupling of the optically generated electric signal with the load, typically for radio frequency (RF) and microwave applications.

Alternatively, when a lateral switch is operated in the nonlinear or filamentary mode, the illumination source is typically a laser diode fed into one or more optical fibers. This mode of operation is considered to have a significant “gain” since the number of conduction electrons and holes is much greater than the number of absorbed photons. A term often used to describe this gain, or filamentary, mode of operation is the lock-on mode (42,43). In this case the fiber output is placed near one of the contact edges that border the switch active region. Then a very short electric pulse is used to drive the laser diode, which in turn produces a short optical pulse to “trigger” the switch to close. This closing sequence results in the formation of a current filament that originates roughly at the point where the laser diode illuminated the switch (87). It has also been shown that multiple current filaments are formed when multiple fibers are used simultaneously to illuminate the switch (88,89). The creation of multiple filaments is intended to increase the switch lifetime since it helps to distribute the current over a larger volume of the semiconductor. Measured lifetimes for filamentary photoconductive switches have been in the range of 10^5 shots to 10^7 shots for devices operating in the range of 10 kV with an active region length of 2.5 mm (86). Larger devices with a 2 cm contact width and a 1.5 cm active region length have demonstrated, in single-pulse experiments, switch voltages as high as 50 kV to 150 kV (86). The lifetimes associated with the larger devices, operating in the gain mode at voltages in excess of 50 kV, are typically much less then the 10^5 shots measured with smaller devices.

Bulk Photoconductive Switches

A second switch geometry that is often used is the bulk geometry, often known as the bulk avalanche semiconductor switch (BASS), shown in Fig. 11. This geometry offers a better hold-off voltage than lateral switches, for a given contact separation, due to the reduced likelihood of surface flashover. The thickness of these devices is normally on the order of 0.5 mm to 1 mm. Therefore, the operating voltage for these type of devices is usually 10 kV or less (90). Bulk devices are more difficult to manufacture since the semiconductor substrate must be processed on both sides. Typically, the top contact, or

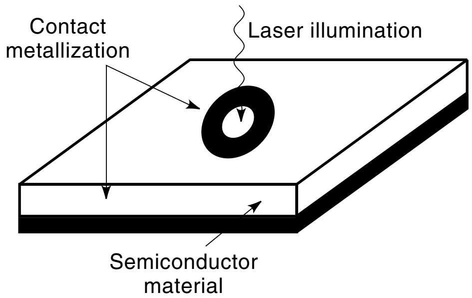

Figure 11. Bulk photoconductive avalanche switch geometry. The longer surface path length between the anode and cathode reduces surface flashover. More stable high voltage operation is achieved.

doughnut contact, is fabricated by either using ion implantation or an epitaxial growth process under the contact metalization. In addition, the laser wavelength that is used to trigger a bulk photoconductive switch must be longer than that used for lateral switches because the carriers must be generated in the interior of the device. For maximum efficiency, the optical absorption depth should be chosen to nearly equal the crystal thickness.

Typically, bulk photoconductive switches are operated in the avalanche mode. A laser diode is used to deliver photons, via a fiber-optic cable, to the hole in the top contact. An optical energy density of only a few nJ/cm^2 is required to trigger a bulk device when the switch is operated at average electric fields on the order of 40 kV/cm to 60 kV/cm (91). Although it is well understood that the avalanche mode is filamentary in nature, the precise mechanisms leading to the controlled breakdown and lock-on of the device are not well understood. Trap filling and impact ionization of traps have been offered as possible explanations for the initiation of lock-on (43,92). In addition, the implications of the geometrical aspects of photoconductive devices have also been theoretically studied in connection with the filamentation process (93).

Bistable Optically Controlled Semiconductor Switch

An alternative switching mechanism was proposed by Schoenbach et al. (9). This concept, called the bistable (or bulk) optically controlled semiconductor switch (BOSS), relies on persistent photoconductivity followed by photoquenching to provide both switch closing and opening, respectively. Persistent photoconductivity results from the excitation of electrons from the deep copper centers found in copper-compensated, silicon-doped, semi-insulating GaAs (GaAs : Si : Cu). The small cross section for electron capture back into the Cu centers allows long conduction times after the first laser pulse is terminated. Photoquenching is accomplished by the application of a second laser pulse of longer wavelength, which ele-

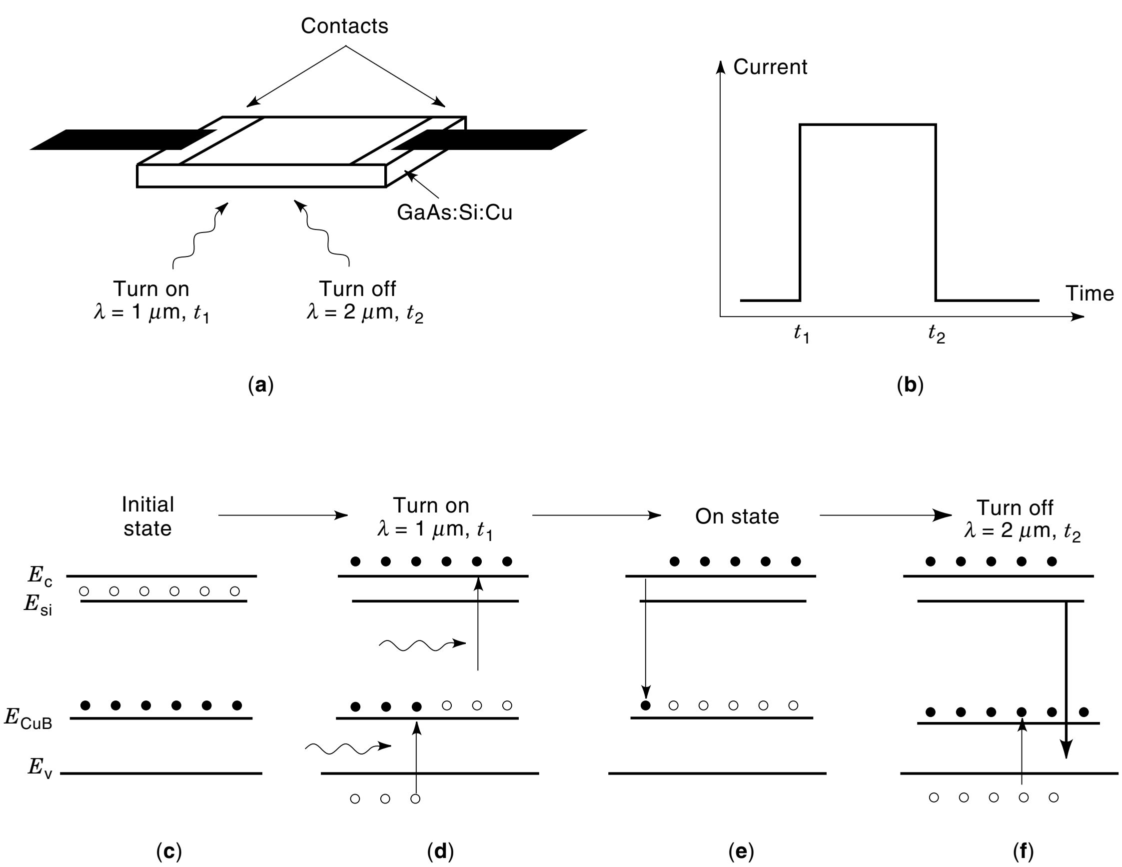

Figure 12. (a) The basic geometry of the BOSS switch, (b) the resulting current delivered to the load during the BOSS switching cycle; (c) the initial high-resistivity state of the material prior to the first laser pulse; (d) the optical excitation of electrons from the Cu_B centers to the conduction band; (e) the slow decay of electrons during the on-state; (f) the fast photo-induced quenching of the photoconductivity.

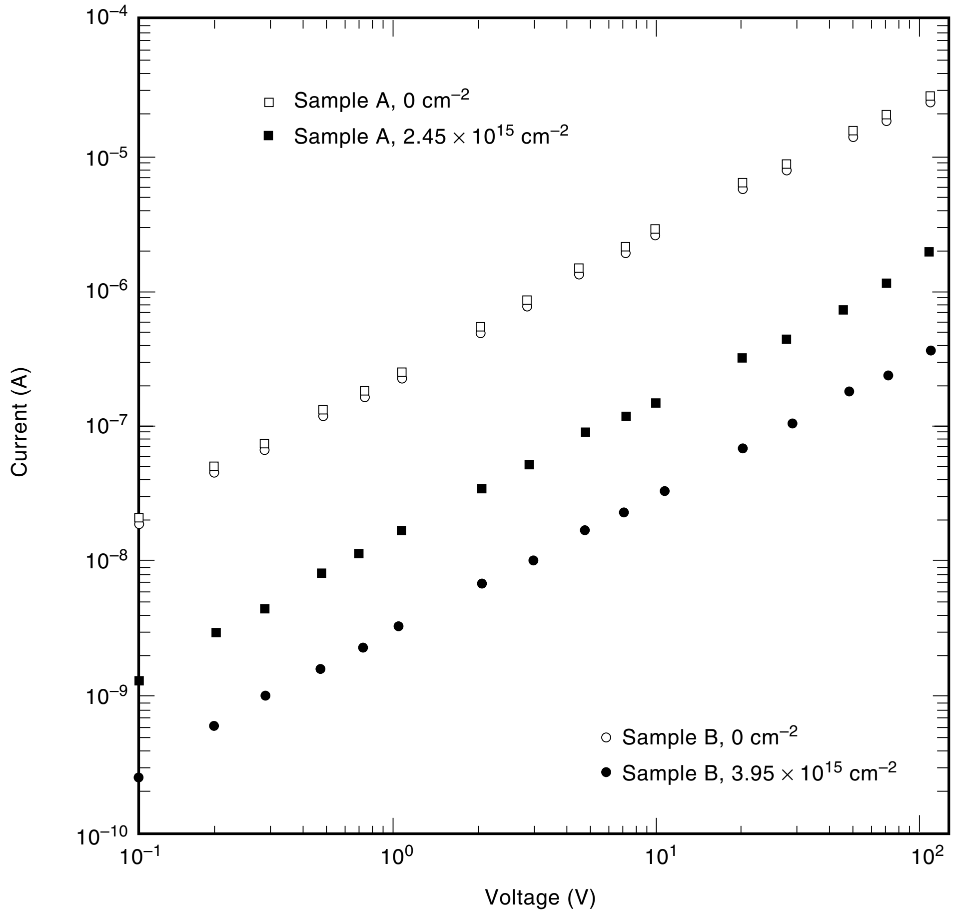

Figure 13. The dc I–V characteristics of BOSS devices before and after neutron irradiation. Samples exposed to higher neutron flux progressively exhibited smaller currents. Differences over three orders of magnitude were experimentally observed.

vates electrons from the valence band back into the copper levels. This laser pulse floods the valence band with free holes, which rapidly recombine with free electrons to quench the photocurrent over a time scale given by the electron–hole lifetime of the material. These processes allow a switch to be developed that can be closed by the application of one laser pulse (1.06 μm) and opened by the application of a second laser pulse with a wavelength about twice that of the turn-on laser. This switching process, as well as the BOSS geometry, is shown in Fig. 12. Note that the switch is illuminated from the back side to help minimize the effects of shadowing by the contact metalization.

Preliminary experimental results showed that the current through a BOSS switch could not be fully quenched by the application of a 140 ps full width at half-maxima (FWHM) 2.13 μm laser pulse. A numerical solution of the semiconductor rate equations for copper-doped GaAs showed that the primary cause for incomplete photoquenching was that the concentration of the recombination centers (RC) was too low (94). As stated previously, the opening transient is the result of a two-step process. The second step is controlled by the electron-hole recombination lifetime in the bulk material. If there is an insufficient RC concentration, the holes that were generated by the 2 μm laser pulse would be retrapped into the copper centers before they could recombine with electrons in the conduction band. This would result in the switch remaining closed after the second laser pulse. Recently, work concentrating on the reduction of the minority-carrier lifetime, by increasing the RC concentration in GaAs, through fast-neutron irradiation was reported by Wang et al. (95). This investigation of neutron damage for the purpose of RC enhancement in BOSS devices was carried further.

Low resistivity, silicon-doped (n-type) GaAs can be made semi-insulating by the introduction of copper acceptor levels through a thermal-diffusion process (96). The GaAs material used in this investigation was originally doped with a silicon concentration of 2×10^{16} cm^{-3} that yielded a resistivity of about 7×10^{-2} Ω-cm. After the thermal diffusion step, at 575°C for 6 h, the samples were polished on both sides to a mirror finish. The sample dimensions were roughly 10 mm by 5 mm by 0.5 mm thick. The p^+–i–n^+ devices were manufactured by depositing a Au–Ge-based metalization for the n-type contact and a Au–Zn-based metalization for the p-type contact. The contacts resulted in switch geometry that was 5 mm wide and separated by a 5 mm gap on the same side of the sample. After deposition, the contacts were annealed at 450°C for 5 min in N_2 at atmospheric pressure. Following the contact anneal, the samples were irradiated with fast neutrons to increase the RC concentration. Two sets of BOSS devices were neutron irradiated at two different fluences. The lower fluence was measured at 2.45×10^{15} cm^{-2} (Sample A) while the higher fluence was measured at 3.93×10^{15} cm^{-2} (Sample B) 1 MeV GaAs equivalent damage (97). The dc I–V characteristics, shown in Fig. 13, of the samples indicated an increase in the switch resistance from about 3.2 MΩ to about 55 MΩ for the lower fluence, and an increase from about 4.3 MΩ to about 273 MΩ for the higher fluence.

The BOSS switching experiments were conducted with a mode-locked Nd:YAG laser system (1.06 μm). It was

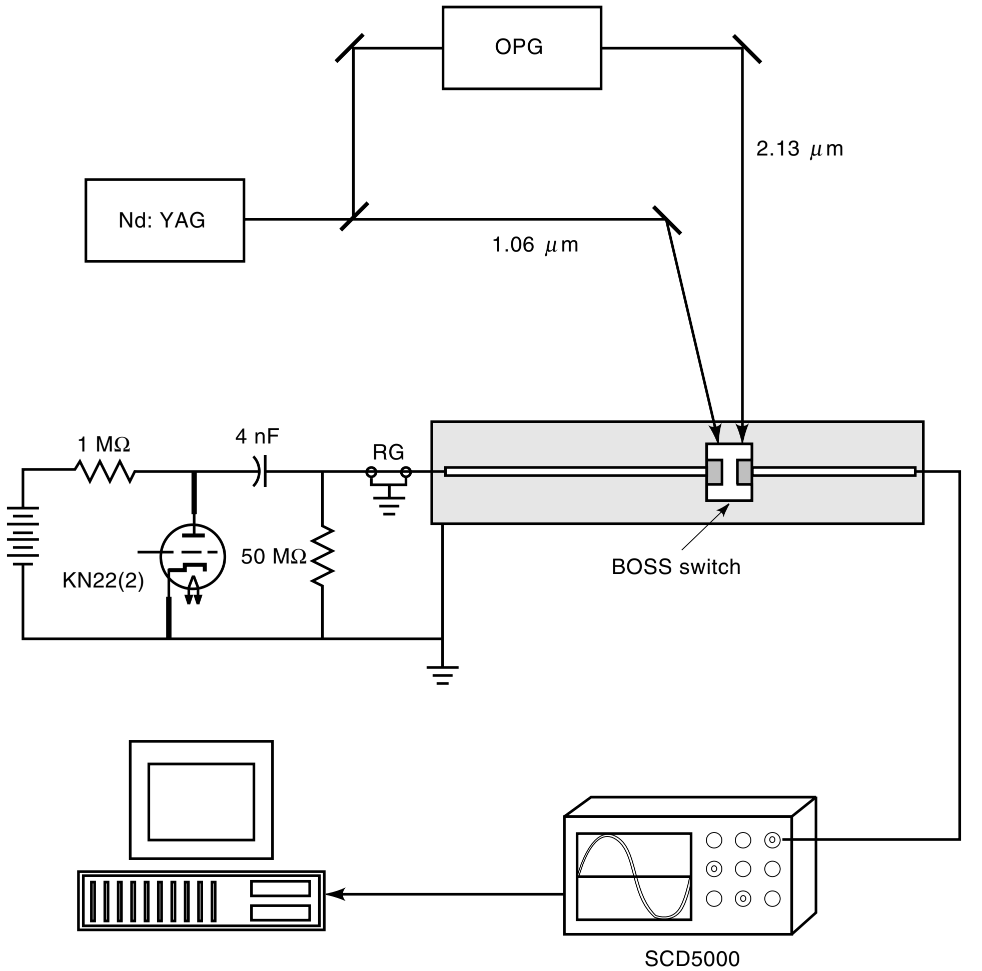

Figure 14. Experimental setup used for performing high-speed and high-power testing of BOSS devices. The switches are shown embedded in a 50 Ω transmission line having a two-way transit time of 8.0 ns. A Klytron produced a 40-ns voltage pulse.

equipped with a optical parametric generator (OPG) that served to double the wavelength (2.13 μm). The laser system produced a Gaussian pulse with a FWHM of about 140 ps. A simple optical delay was then used to adjust the time between switch closure and when the switch was opened. Photoconductivity measurements were performed to evaluate the operation of the neutron irradiated BOSS devices. The BOSS switches were embedded in a 50 Ω transmission line (two-way transit time 8 ns) that was pulse charged with roughly a 40 ns FWHM voltage pulse generated by a Krytron switch, as shown in Fig. 14. The maximum voltage applied to the BOSS devices was about 18 kV.

Lower-Fluence Switching Results. Switching results illustrating the photocurrent for Sample A are shown in Fig. 15 for an applied voltage of 3.7 kV. The maximum voltage that was switched with this device was about 18 kV, which was bias-voltage modulator limited. The switching behavior of Sample A did not change as the applied voltage was increased. Figure 15 shows several current waveforms superimposed to demonstrate the ability to control the pulse width of the electrical pulse. The laser pulse energy for both the wavelengths was set at 4.5 mJ. Figure 15 illustrates that as the time between the two laser pulses is increased, the switch conductivity decreases with time prior to the turn-off laser pulse as a result of the enhanced RC density. This effect will ultimately limit the switch on time of neutron-irradiated BOSS devices. Therefore, there appears to be a tradeoff between the maximum time that the switch will remain closed after the 1.06 μm laser pulse and the RC density in the material. It should be noted that BOSS devices that were not irradiated with neutrons had demonstrated on times of several hundred nanoseconds (98).

When the time between laser pulses is too short, the 2 μm laser pulse is no longer able to quench the photocurrent. Eventually, when the two laser pulses are roughly coincident, the switch will behave as if there was no 2 μm laser pulse at all. It takes a certain amount of time for the electron-hole plasma generated by the 1 μm laser pulse to recombine. This, coupled with the fact that the dominant copper center (Cu_B) requires a certain amount of time to fill with a sufficient quantity of holes to permit complete photoquenching, sets a lower limit on the time between the turn-on and turn-off laser pulses.

Higher-Fluence Switching Results. Photoconductivity experiments were also conducted on Sample B, which was irradiated at a fluence of 3.93×10^{15} cm^{-2}. One drawback of an increased RC concentration is that the on-state conductivity will be reduced because electrons in the conduction band will recombine with holes in the valence band before those holes can be trapped in the Cu_B center. This process reduces the number of holes that are trapped in the Cu_B center, which in turn reduces the available sites to receive electrons from the

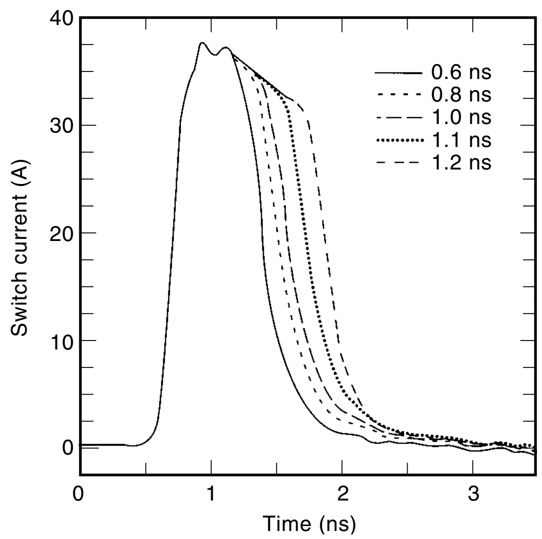

Figure 15. Demonstration of electric pulse-width agility through variations in the time delay between the turn-on and turn-off laser pulses. The applied voltage was 3.7 kV. Though neutron irradiation helped attain electrical pulses as short as 1.0 ns, waveform distortion set in for longer durations.

valence band during the turn-off laser pulse. However, a benefit can be derived if the RC concentration in the bulk material is made high enough to cause the switch to open without the need of the turn-off laser pulse. This effect is shown in Fig. 16, where two 1.06 μm laser pulses were used to close Sample B at a high repetition rate. For these experiments, the switch was only illuminated by two 1 μm laser pulses with a variable time delay between them. The reason Sample B opened without the turn-off laser pulse was because it was irradiated at a higher neutron fluence than Sample A. Therefore, there was a higher RC density in the bulk material of Sample B. The purpose of this experiment was twofold: First,

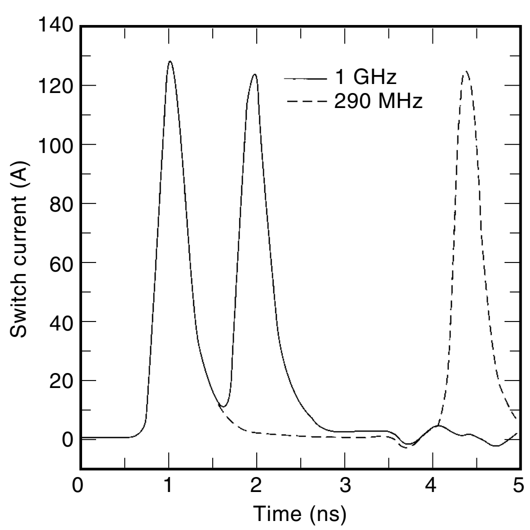

Figure 16. Experimental demonstration of 1 GHz and 290 MHz repetition rates within an optical two-pulse burst at an applied voltage of 16 kV. The high recombination rates in neutron irradiated samples allowed for such fast turn off. The 340-ps pulse widths measured are among the shortest for high power semiconductor switches.

we wanted to see how the switch responded to the turn-on laser pulse; and second, we wanted to test the repetition rate capability of Sample B. The applied voltage for the waveform shown in Fig. 16 was about 16 kV. The average pulse width was measured to be about 340 ps. As shown in Fig. 16, the time separation between the two laser pulses varied from about 3.5 ns, corresponding to a repetition rate of roughly 290 MHz, down to roughly 1 ns, corresponding to a repetition rate of 1 GHz. These repetition rates are basically five orders of magnitude higher than any other type of high-power photoconductive switch. The maximum voltage that was switched with this device was 18 kV, yielding an average electric field of 36 kV/cm.

It is important to note that there was no indication of the device collapsing into a filamentary-current mode, or lock-on mode, of conduction at any point in the switching cycle. This is significant since almost all previously reported photoconductive switching experiments on non-neutron-irradiated GaAs, including those performed on GaAs : Si : Cu material, exhibited a transition into filamentary conduction at average electric fields of about 10 kV/cm (99). It has been reported by Loubriel et al. (100), however, that chrome-doped GaAs switches, which were irradiated at a neutron fluence of 5×10^{15} cm^{-2}, did not transition into a filamentary conduction mode until the applied average electric field was greater than 62 kV/cm. This electric field would correspond to an operating voltage of roughly 30 kV for the 5 mm gap BOSS devices. The most striking attribute of the current pulses in Fig. 16 is that the switch completely opens without the need of the 2 μm laser pulse.

BOSS-Based RF Sources. The primary goal of this research is to produce a wideband, frequency-agile source that can radiate the RF energy with a broadband antenna. To maximize the radiative efficiency of the source, it is necessary to produce ac power, thereby reducing the dc component of the waveform, which cannot be radiated. The ability of the BOSS switch to open, as well as close, in the subnanosecond regime allows a new type of RF source to be developed that is capable of generating repetitive high-power microwave cycles of varying duration, depending on the relative delay between the turn-on and turn-off laser pulses. A source configuration that is capable of generating ac power with real-time frequency agility is shown in Fig. 17 and is called the pulse-switch-out (PSO) generator. This source uses two BOSS switches that are embedded in oppositely charged 50 Ω transmission lines, which can generate single positive and negative half-cycles by first closing and opening each switch. Both switches then feed into a single 50 Ω transmission line that leads to a matched load.

Experiments were conducted with the circuit shown in Fig. 17 at a bias voltage of about 9.5 kV, and with BOSS devices that were irradiated at the higher neutron fluence and therefore only illuminated with 1 μm laser pulses. Experiments will be conducted shortly with devices that require both of the laser pulses. The time-domain waveforms for a time delay of about 500 ps and about 2 ns are shown in Fig. 18. We found that the pulse width of the positive half-cycle could be reduced, at the expense of the negative half-cycle peak voltage, by closing the second BOSS switch before the first one was completely open. The Fourier spectra for these two waveforms differ significantly, as shown in Fig. 19. As expected, the bipo-

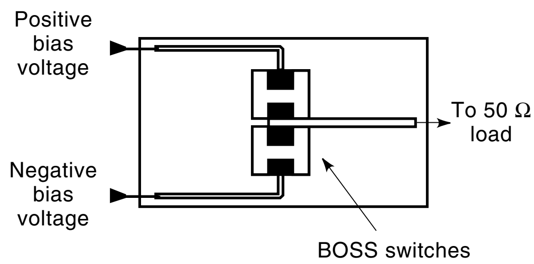

Figure 17. Stripline configuration of the pulse-switch-out (PSO) generator. In this setup, the switches were used for producing a wide-band, frequency agile source for RF energy radiation through broad-band antennas.

lar pulses significantly reduced the dc component in the spectra. In addition, the generation of nulls in the spectra increased the power spectral density at some of the lower frequencies. The number and location of these nulls can be adjusted by varying the time delay between the two laser pulses.

GaAs Optothyristors

Ordinary thyristors are bulk current-controlled switching devices with kiloampere current-carrying capabilities and blocking voltages in the kilovolt range. However, their turn-on speeds are relatively slow since a regenerative feedback mechanism based on internal space-charge layer modulation is responsible for the switching action (76). Similarly, the turn-off characteristics are generally limited by the characteristic electron-hole recombination times. To enhance the response and increase the voltage scaling capability, AlGaAs-SI GaAs optothyristor switch structures have been suggested (11). Such optically triggered thyristor switches gained attention when high-voltage direct current transmission was considered as a viable and cost-effective alternative to the ac transmission over long distances. The conventional thyristors had to be stacked serially to attain the desired hold-off capabilities, which led to complex triggering and control electrical

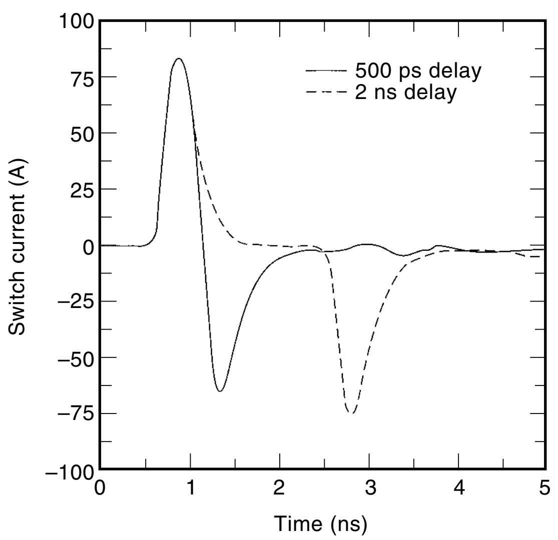

Figure 18. Experimental demonstration of two bipolar pulses produced by a PSO generator for 500-ps and 2-ns delays between the 1 μm laser pulses.

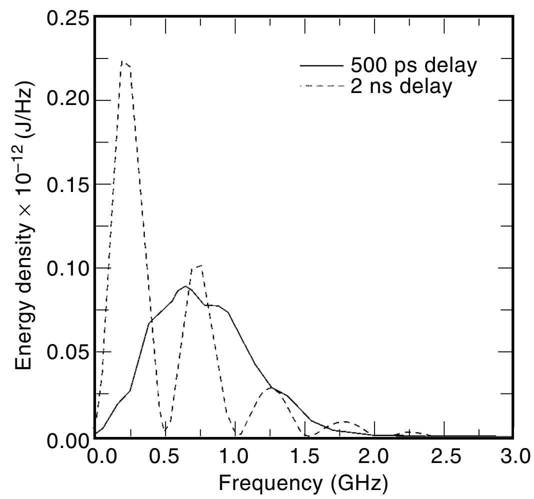

Figure 19. Fourier spectra of the two waveforms shown in Fig. 18. The existence of the bipolar swing significantly reduced the dc component in the spectra. By varying the optical excitation pulse delay, the spectra could be altered as desired.

circuitry. However, optical triggering successfully isolated the switching device from the control circuitry. The turn-on times could be dramatically reduced as the photogeneration process provided for large increases in the current. Finally, the use of SI-GaAs as a sandwich layer between doped AlGaAs region led to P^+-AlGaAs/N-AlGaAs-/SI-GaAs-/P-AlGaAs-/N^+-AlGaAs structures capable of flexible voltage scaling. Advantages of such a optothyristor structures include (1) a natural wavelength-dependent absorption window within the SI GaAs region for the triggering; (2) more uniform current densities due to the formation of a near-homogeneous electron-hole plasma (geometric effects of contact and current crowding can be reduced through optical turn-on); (3) faster turn-on times; and (4) hold-off voltage flexibility through variations in the thickness of the SI-GaAs layer.

While promising in some respects, the optothyristor has revealed problems of lock-on and catastrophic failure through current filamentation at high voltages. These problems, though not well understood, are likely to arise from the SI-GaAs layer and the deep defects therein. All of the transport physics described previously should apply. Also, unlike the BOSS switch, the optothyristor is not inherently an "opening" switch, and the turn-off cannot be controlled in a flexible manner. Recombination centers and traps have to be introduced to enhance turn-off times, which are on the order of a hundred nanoseconds.

Optically Switched MESFET Devices

Metal-oxide-semiconductor field-effect transistors (MESFET) have also recently been proposed as elements for optically activated switching. Such structures have been used as optical detectors (101) and photomixers (102). The basic concept involves photogeneration of carriers in the region between the source and drain contacts to produce a current output as these mobile charges move along the channel. Some of the obvious benefits associated with switching in such a structure include the following:

1. Shorter carrier traversal times as the mobile charge is created between the source and drain regions. However,

the source-drain distance cannot be made very small to take advantage of "ballistic transport" (103) since a sufficiently large optical illumination area and hold-off voltage capability has to be maintained.

2. The possibility of controlling the photocurrent through variations in the input wavelength. Lower wavelengths have been shown to increase current due to the combined effect of a larger density of states at the higher optical energies for enhanced absorption and the higher initial carrier velocities.
3. Photoexcitation-controlled enhancement in the effective channel depth that allows for larger current throughput. The increase in the channel area is due to a photovoltaic effect that works to reduce the potential barrier between the semi-insulating substrate and the conducting epilayer. As a result, the electron-hole plasma tends to flow not only within the channel but also partially within the SI substrate.
4. More efficient heat dissipation through the metallic gate, which helps improve thermal management.

However, a number of potential drawbacks are expected to restrict the utility of optically activated MESFET switches. For instance, the MESFET is a relatively more complicated structure than the simple bulk photoconductor discussed previously, which is a disadvantage. Moreover, hold-off voltages of such MESFETs are far smaller than the other bulk devices, such as the BOSS and the BASS. This arises from the two-dimensional shape of the depletion layer and resulting carrier tunneling at large values of the applied drain bias. In addition, the presence of a gate contact introduces additional parasitics. The turn-off speeds can therefore be expected to be slow. Finally, the photovoltaic effect, which leads to a reduction in the channel-substrate barrier, introduces an additional current flow perpendicular to the longitudinal channel. The source-substrate-drain regions behave in a manner analogous to that of a phototransistor with a floating base. Some fraction of the photogenerated holes moves toward the gate and is collected, while electrons enter the substrate region. This gives rise to a substantial gate current, which can effectively lower the conversion efficiency and divert the current flow from the drain. Usually, a large gate resistance is necessary to minimize such gate currents. However, this comes at the price of lower response speed. The opto-MESFET switches fabricated and tested to date have been found to be useful only over time intervals spanning the submicrosecond regime and higher (12).

Furthermore, the MESFET devices are expected to suffer from problems of internal dipole layer formation and high field domains between the gate-drain regions, as in regular MESFET structures (104). Finally, the presence of bipolar current conduction through the SI-GaAs layer can lead to all of the deep-level instability problems discussed previously and worsen the noise figure.

BIBLIOGRAPHY

1. I. V. Grekhov, New principles of high power switching with semiconductor devices, *Solid State Electronics,* **32**: 923–930, 1989.
2. Special Issue, *IEEE Trans. Elec. Dev.,* **ED-37**: 242–673, 1990.
3. G. Schaefer, M. Kristiansen, and A. Guenther, in *Gas Discharge Closing Switches,* New York: Plenum Press, 1990.
4. B. Jayant Baliga, in *Power Semiconductor Devices,* Boston: PWS Publishers, 1996; B. Jayant Baliga, in *Modern Power Devices,* New York: Wiley, 1987.
5. R. S. Ramshaw, in *Power Electronics Semiconductor Switches,* London: Chapman & Hall, 1993.
6. R. A. Kiehl, "An Avalanching Optoelectronic Microwave Switch," *IEEE Trans. Microw. Theory Tech.,* **MTT-27**: 533–539, 1979.
7. I. V. Grekhov et al., Initial stages of the growth of the impact ionization of waves in *p-n* junctions subject to overvoltages, *Sov. Phys. Semicond.,* **17**: 877–880, 1983.
8. I. V. Grekhov et al., Formation of nanosecond high-voltage drops across semiconductor diodes with voltage recovery by a drift mechanism, *Sov. Tech. Phys. Lett.,* **9**: 188–190, 1983; I. V. Grekhov et al., Initiation of breakdown of *p-n* junctions subjected to overvoltage, *Sov. Phys. Tech. Phys.,* **26**: 984–985, 1981.
9. K. H. Schoenbach et al., An optically controlled closing and opening semiconductor switch, *J. Appl. Phys.,* **63**: 2460–2463, 1988.
10. K. H. Schoenbach et al., Electron-beam controlled high power semiconductor switches, *IEEE Trans. Elec. Dev.,* **ED-36**: 1793–1802, 1989.
11. J. Zhao et al., A novel high power optothyristor based on AlGaAs/GaAs for pulsed power switching, *IEEE Trans. Elec. Dev.,* **ED-41**: 819–825, 1994.
12. A. Madjar and P. Herczfeld, The GaAs MESFET as an optically activated switch, in A. Rosen and F. Zutavern (eds.), *High Power Optically Activated Solid-State Switches,* Boston: Artech House, 1994, pp. 187–217.
13. *Solid State Electronics,* **32**: 1051–1954, 1989.
14. W. C. Nunnally, Linear photoconductive power switches, in A. Rosen and F. Zutavern (eds.), *High Power Optically Activated Solid-State Switches,* Boston: Artech House, 1994, pp. 29–42.
15. A. Rose, in *Concepts in Photoconductivity and Allied Problems,* New York: Krieger, 1963.
16. Y. Marfaing, in *Handbook on Semiconductors,* C. Hilsum (ed.), Amsterdam: North-Holland, 1981, Vol. 2, Chap. 7, pp. 671–709.
17. A. J. DeMaria et al., Picosecond laser pulses, *Proc. IEEE 57,* pp. 2–25, 1969.
18. C. H. Lee, "Introduction: A Historical Overview," in C. H. Lee (ed.), *Picosecond Optoelectronic Devices,* Orlando: Academic Press, 1984, pp. 1–9.
19. *Picosecond Optoelectronic Devices,* C. H. Lee (ed.), Orlando: Academic Press, 1984, pp. 1–406.
20. D. H. Auston, Picosecond optoelectronic switching and gating in silicon, *Appl. Phys. Lett.,* **26**: 101–103, 1975.
21. P. Lefur and D. H. Auston, A kilovolt picosecond optoelectronic switch and Pockel's cell, *Appl. Phys. Lett.,* **28**: 21–23, 1976.
22. D. H. Auston, Picosecond photoconductors: Physical properties and applications, in C. H. Lee (ed.), *Picosecond Optoelectronic Devices,* Orlando: Academic Press, 1984, pp. 73–117.
23. G. Mourou and W. Knox, High-power switching with picosecond precision, *Appl. Phys. Lett.,* **35**: 492–495, 1979.
24. G. Mourou, W. Know, and S. Williamson, Advances in picosecond optoelectronics, *Proc. of the SPIE—The International Society for Optical Engineering,* **322**: 107–114, 1982.
25. C. H. Lee, P. S. Pak, and A. P. DeFonzo, Optical control of millimeter-wave propagation in dielectric waveguides, *IEEE Journal of Quantum Electronics,* **QE-16**: 277–288, 1980.
26. Picosecond optoelectronic switching in $CdS_{0.5}Se_{0.5}$, *Optics Comm.,* **32**: 485–488, 1980.
27. J. A. Valdmanis and G. Mourou, Subpicosecond electro-optic sampling: Principles and applications, *IEEE J. Quantum Electronics,* **QE-22**: 69–78, 1986.

28. Y. Chen et al., 375-GHz-bandwidth photoconductive detector, *Appl. Phys. Lett.,* **59**: 1984–1986, 1991.

29. J. Agostinelli, G. Mourou, and C. W. Gabel, Active pulse shaping in the picosecond domain, *Appl. Phys. Lett.,* **35**: 731–733, 1979.

30. M. Stavola, J. Agostinelli, and M. Sceats, Ultrafast pulse shaping with a traveling wave Kerr cell and picosecond rise time electrical pulses, *Appl. Opt.,* **18**: 4101–4105, 1979.

31. W. Margulis et al., Reduction of jitter in streak-camera synchronization with picosecond laser pulses, *Opt. Commun.,* **32**: 331–333, 1980.

32. H. Yoshida et al., Intersubband transitions in InGaAs/AlAs coupled double quantum well structures for multi-wavelength all-optical switching, *Electron. Lett.,* **34**: 913–915, 1998.

33. C. Knorr et al., A mechanism for low-power all-optical switching in multiple quantum-well structures, *Appl. Phys. Lett.,* **69**: 4212–4214, 1996.

34. A. Tacheuchi et al., Picosecond all-optical switching using tunneling and spin-relaxation in quantum well structures, *Optoelectronics—Devices and Technologies,* **10**: 561–574, 1996.

35. H. R. Fetterman, Lightwave-terahertz interaction, in J. M. Chamberlain and R. E. Miles (eds.), *New Directions in Terahertz Technology,* Netherlands: Kluwer Academic, 1997, pp. 343–358.

36. S. Schmitt-Rink et al., Prospects for THz quantum well optoelectronics, *Proceedings of the SPIE—International Society for Optical Engineering,* **1216**: 53–62, 1990.

37. D. A. B. Miller, Quantum well optoelectronic switching devices, *Int. J. High Speed Electr.,* **1**: 19–46, 1990.

38. W. H. Weber, Double injection in long *p-i-n* diodes with deep double acceptors, *Appl. Phys. Lett.,* **16**: 396–399, 1970.

39. M. A. Lampert and P. Mark, in *Current Injection in Solids,* New York: Academic Press, 1970.

40. R. H. Bube, in *Photoelectric Properties of Semiconductors,* Cambridge: Cambridge Press, 1992.

41. F. Capasso, Bandgap engineering: From physics and materials to new semiconductor devices, *Science,* **235**: 172–176, 1987.

42. G. M. Loubriel, M. W. O'Malley, and F. J. Zutavern, Toward pulse power uses for photoconductive semiconductor switches: Closing switches, *Proc. 6th IEEE Pulsed Power Conf.,* Arlington, VA, pp. 145–148, 1987; F. J. Zutavern et al., Photoconductive semiconductor switch experiments for pulsed power applications, *IEEE Trans. Elec. Dev.,* **ED-37**: 2472–2477, 1990.

43. R. P. Brinkmann et al., The lock-on effect in gallium arsenide switches, *IEEE Trans. Elec. Dev.,* **ED-38**: 701–704, 1991.

44. S. Sheng et al., An investigation of 3C-SiC photoconductive switching devices, *Mater. Science and Engr. B,* **46**: 147–151, 1997.

45. P. T. Ho and J. Goldhar, Photoconductive switching using diamond and zinc selenide, in *High Power Optically Activated Solid-State Switches,* Boston: Artech House, 1994, pp. 81–93.

46. S. T. Feng, P. T. Ho, and J. Goldhar, Photoconductive switching using polycrystalline ZnSe, *IEEE Trans. Elec. Dev.,* **ED-37**: 2517–2519, 1990.

47. J. W. Palmour et al., 6H-SiC devices and applications, *Physica B,* **185**: 461–465, 1993.

48. M. S. Mazzola et al., GaAs photoconductive closing switches with dark resistance and microsecond conductivity decay, *Appl. Phys. Lett.,* **54**: 20–22, 1989.

49. D. V. Lang, Deep level transient spectroscopy: A new method to characterize traps in semiconductors, *J. Appl. Phys.,* **45**: 3023–3032, 1974.

50. C. Hurtes et al., Deep level spectroscopy in high-resistivity materials, *Appl. Phys. Lett.,* **32**: 821–823, 1978.

51. A. L. Lin, E. Omelianovski, and R. H. Bube, Photoelectric properties of high resistivity GaAs, *J. Appl. Phys.,* **47**: 1852–1858, 1976.

52. D. V. Lang, Space-charge spectroscopy in semiconductors, in *Topics in Applied Physics: Thermally Stimulated Relaxation in Solids,* Berlin: Springer, 1979, **37**: 93–133.

53. D. C. Stoudt, R. P. Brinkmann, and R. A. Roush, Subnanosecond high power performance of a bistable optically controlled GaAs switch, in *GaAs and Related Compounds: Proc. 20th International Conference (IOP, Bristol, UK, 1994), Institute of Physics Conf. Series,* **136**: 325–328.

54. A. G. Milnes, in *Deep Impurities in Semiconductors,* New York: Wiley, 1973.

55. N. Y. Mott and R. W. Gurney, in *Electronic Processes in Ionic Crystals,* Oxford Univ. Press, Clarendon, 1940, p. 62.

56. K. Kitahara et al., Electrical and photoelectronic properties of Cr-doped GaAs, *J. Appl. Phys.,* **50**: 5339–5343, 1979.

57. D. C. Stoudt, in *The Electrical Characterization of Semi-Insulating Galium Arsenide: A Material for High Power Switches,* Thesis, Old Dominion University, 1989.

58. G. M. Martin, A. Mitonneau, and A. Mircea, Electron traps in bulk and epitaxial GaAs crystals, *Electr. Lett.,* **13**: 191–193, 1977.

59. G. M. Martin et al., Compensation mechanisms in GaAs, *J. Appl. Phys.,* **51**: 2840–2852, 1980.

60. D. C. Stoudt et al., The recovery behavior of semi-insulating GaAs switches, *IEEE Trans. Elec. Dev.,* **ED-37**: 2478–2485, 1990.

61. Zh. I. Alferov et al., Investigation of S-type diodes made of chromium-doped semi-insulating GaAs, *Sov. Phys. Semicond.,* **4**: 1742–1748, 1970.

62. R. A. Roush, K. H. Schoenbach, and R. P. Brinkmann, Bistable behavior of the dark current in copper-doped semi-insulating gallium arsenide, *J. Appl. Phys.,* **71**: 4354–4356, 1992.

63. V. A. Brodovoi, A. Ch. Gozak, and G. P. Peka, Negative resistance of symmetric GaAs : Cr structures, *Sov. Phys. Semicond.,* **8**: 223–225, 1974.

64. L. Borghi, P. De Stefano, and P. Mascheretti, Photoconductivity of neutron irradiated gallium arsenide, *J. Appl. Phys.,* **41**: 4665–4668, 1970.

65. D. C. Stoudt et al., Effects of 1 MeV neutron radiation on the operation of a bistable optically controlled semiconductor switch, *IEEE Trans. Elec. Dev.,* **ED-41**: 913–919, 1994.

66. S. L. Huang et al., Comparison of oxygen and proton implanted GaAs photoconductive switches, *OSA Proc. Picosecond Electronics and Optoelectronics,* edited by T. C. L. Sollner and J. Shah (OSA Press, New York, 1991), Vol. 9, pp. 248–252.

67. R. A. Falk et al., Electrooptic imagery of high voltage GaAs photoconducting switches, *IEEE Trans. Elec. Dev.,* **ED-42**: 43–49, 1995.

68. E. F. Schubert, A. Fischer, and K. Ploog, Photoconductivity in *n*- and *p*-doped AlGaAs heterostructures, *Solid St. Electronics,* **29**: 173–180, 1986.

69. H. J. Queisser and D. E. Theodorou, Hall effect analysis of persistent photocurrents in *n*-GaAs layers, *Phys. Rev. Lett.,* **43**: 401–404, 1979.

70. J. Klem et al., Persistent photoconductivity in AlGaAs/GaAs modulation doped structures: Dependence on structure and growth temperature, *J. Appl. Phys.,* **54**: 5214–5217, 1983.

71. R. Fletcher et al., Persistent photoconductivity and two-band effects in GaAs/AlGaAs heterojunctions, *Phys. Rev. B,* **41**: 10649–10666, 1990.

72. T. Frello, E. Veje, and O. Leistiko, Observation of time varying and persistent photoconductivity in porous silicon, *J. Appl. Phys.,* **79**: 1027–1031, 1996.

73. H. M. Chen et al., Persistent photoconductivity in *n*-type GaN, *J. Appl. Phys.,* **82**: 899–901, 1997.
74. C. H. Qiu and J. I. Pankove, Deep levels and persistent photoconductivity in GaN thin films, *Appl. Phys. Lett.,* **70**: 1983–1985, 1997.
75. D. E. Lacklison et al., A comparison of photoconduction effects in AlGaAs and GaAs heterostructures, *Semicond. Sci. Technol.,* **3**: 663–640, 1988.
76. S. M. Sze, in *Physics of Semiconductor Devices,* New York: Wiley, 1981.
77. R. T. Tung et al., Schottky barrier inhomogeneity at epitaxial $NiSi_2$ interfaces on Si(100), *Phys. Rev. Lett.,* **66**: 72–75, 1991.
78. R. J. Hauenstein et al., Schottky barrier height measurements of epitaxial $NiSi_2$ on Si, *Appl. Phys. Lett.,* **47**: 853–855, 1985.
79. J. L. Freeouf et al., Size dependence of effective barrier heights of mixed phase contacts, *J. Vac. Sci. Technol.,* **21**: 570–573, 1982.
80. J. H. Werner and H. H. Guttler, Barrier inhomogeneities at Schottky contacts, *J. Appl. Phys.,* **69**: 1522–1533, 1991; A. J. Madenach and J. H. Werner, Noise spectroscopy of silicon grain boundaries, *Phys. Rev. B,* **38**: 13150–13162, 1988.
81. M. D. Pocha and R. L. Druce, 35 kV GaAs nanosecond photoconductive switches, *IEEE Trans. Elec. Dev.,* **ED-37**: 2486–2492, 1990.
82. J. B. Gunn, Instabilities of current in III-V semiconductors, *IBM J. Res. Dev.,* **8**: 141–147, 1964.
83. B. K. Ridley and T. B. Watkins, *Proc. Phys. Soc. London,* **78**: 293, 1961; B. K. Ridley, Anatomy of the transferred electron effect in III-V semiconductors, *J. Appl. Phys.,* **48**: 754–764, 1977.
84. B. L. Gelmont and M. S. Shur, S-type current voltage characteristics in Gunn diodes, *J. Phys. D. Appl. Phys.,* **6**: 842–850, 1973.
85. *High Power Optically Activated Solid-State Switches,* edited by A. Rosen and F. Zutavern, Boston: Artech House, 1994.
86. F. J. Zutavern and G. M. Loubriel, High-voltage lateral switches from silicon or gallium arsenide, in A. Rosen and F. Zutavern (eds.), *High Power Optically Activated Solid-State Switches,* Boston: Artech House, 1994, pp. 245–296.
87. F. J. Zutavern et al., Electrical and optical properties of high gain GaAs switches, in *Optically Activated Switching II, Proc. SPIE* **1632**, Los Angeles, CA, pp. 152–159, 1992.
88. F. J. Zutavern et al., Characteristics of current filamentation in high gain photoconductive semiconductor switching, *Proc. 20th IEEE Power Modulator Symposium,* Myrtle Beach, SC, pp. 305–311, 1992.
89. F. J. Zutavern et al., Optically controlled current filamentation in GaAs photoconductive semiconductor switches, *Proc. 9th IEEE Pulsed Power Conference,* Albuquerque, NM, pp. 80–83, 1993.
90. M. D. Pocha et al., Avalanche photoconductive switching, *Proc. 7th IEEE Pulsed Power Conference,* Monterey, CA, pp. 866–868, 1989.
91. M. D. Pocha, R. L. Druce, and W. W. Hofer, High voltage, subnanosecond photoconductive switching, UCRL 53868-89, available from U.S. Dept. of Commerce Technical Report, 5285 Port Royal Road, Springfield, VA 22161.
92. R. L. Druce et al., Photoconductive switching in GaAs, in *Engineering Research Development in Technology: FY 91,* Livermore, CA: Lawrence Livermore National Laboratory, 1992, pp. 6.1–6.12.
93. R. P. Brinkmann, Filamentation in optically controlled semiconductor switches, *Proc. 9th IEEE Pulsed Power Conference,* Albuquerque, NM, pp. 665–667, 1993.
94. D. C. Stoudt, R. P. Brinkmann, and R. A. Roush, Subnanosecond high power performance of a bistable optically controlled GaAs switch, *Proc. of Intl. Symp. on GaAs and Related Compounds (IOP, Bristol, UK, 1993), Institute of Physics Conf. Series,* **136**, pp. 325–328.
95. C. L. Wang, M. D. Pocha, and J. D. Morse, Neutron treated, ultrafast photoconductor detectors, *Appl. Phys. Lett.,* **54**: 1451–1453, 1989.
96. R. A. Roush, D. C. Stoudt, and M. S. Mazzola, Compensation of shallow silicon donors by deep copper acceptors in gallium arsenide, *Appl. Phys. Lett.,* **62**: 2670–2672, 1993.
97. P. J. Griffin et al., Neutron damage equivalence in GaAs, *IEEE Trans. Nuclear Sci.,* **38**: 1216–1224, 1991.
98. D. C. Stoudt et al., Investigation of a laser controlled copper doped GaAs closing and opening switch for pulsed power applications, *Proc. 8th IEEE Pulsed Power Conference,* San Diego, CA, 41–44, 1991.
99. M. S. Mazzola et al., Evaluation of transport effects on the performance of a laser-controlled GaAs switch, *Proc. 8th IEEE Pulsed Power Conference,* San Diego, CA, 37–44, 1991.
100. G. M. Loubriel et al., Closing photoconductive semiconductor switches, *Proc. 7th IEEE Pulsed Power Conference,* Monterey, CA, 45–59, 1989.
101. C. Baack, G. Elze, and G. Walf, GaAs MESFET: a high speed optical detector, *Electr. Lett.,* **13**: 7–8, 1977.
102. C. C. Ni, H. Fetterman, and W. Chew, Millimeter wave generation and characterization of a GaAs FET by optical mixing, *IEEE Trans. Microwave Theory and Techniques,* **MTT-38**: 608–614, 1990.
103. M. S. Shur and L. F. Eastman, Ballistic transport in semiconductors at low temperatures for low power, high speed logic, *IEEE Trans. Elec. Dev.,* **ED-26**: 1677–1683, 1979.
104. C. A. Liechti, Microwave Field Effect Transistors, *IEEE Trans. Microwave and Techniques,* **MTT-24**: 279–300, 1976.

R. P. Joshi
Old Dominion University

D. C. Stoudt
Naval Surface Warfare Center

PHOTOCONDUCTIVE CELL. See Photoresistors.